RL-TR-96-287
Final Technical Report
April 1997

SELF COHERING AN OTH RADAR ON CLUTTER RETURNS

Gorca Systems, Inc.

Hesham Attia, Kenneth Abend, Barry Fell

19970707 062

DTIC QUALITY INSPECTED 3

**Rome Laboratory
Air Force Materiel Command
Rome, New York**

Although this report references limited document RADC-TR-89-296, no limited information has been extracted.

This report has been reviewed by the Rome Laboratory Public Affairs Office (PA) and is releasable to the National Technical Information Service (NTIS). At NTIS it will be releasable to the general public, including foreign nations.

RL-TR-96-287 has been reviewed and is approved for publication.

APPROVED:

DAVID S. CHOI
Project Engineer

FOR THE COMMANDER:

ROBERT V. MCGAHAN, Acting Director
Electromagnetics and Reliability Directorate

REPORT DOCUMENTATION PAGE

Public reporting burden for this collection of information is estimated to average 1 hour per response, including the time for reviewing instructions, searching existing data sources, gathering and maintaining the data needed, and completing and reviewing the collection of information. Send comments regarding this burden estimate or any other aspect of this collection of information, including suggestions for reducing this burden, to Washington Headquarters Services, Directorate for Information Operations and Reports, 1215 Jefferson Davis Highway, Suite 1204, Arlington, VA 22202-4302, and to the Office of Management and Budget, Paperwork Reduction Project (0704-0188), Washington, DC 20503.

1. AGENCY USE ONLY *(Leave blank)*	2. REPORT DATE	3. REPORT TYPE AND DATES COVERED
	April 1997	FINAL - Jun 92 - Sep 94

4. TITLE AND SUBTITLE

SELF COHERING AN OTH RADAR ON CLUTTER RETURNS

5. FUNDING NUMBERS

C - F19628-92-C-0024
PE - 62702F
PR - 4600
TA - 16
WU - 86

6. AUTHOR(S)

Heshman Attia, Kenneth Abend, and Barry Fell

7. PERFORMING ORGANIZATION NAME(S) AND ADDRESS(ES)

Gorca Systems, Inc.
PO Box 2325
Cherry Hill, NJ 08034

8. PERFORMING ORGANIZATION REPORT NUMBER

N/A

9. SPONSORING/MONITORING AGENCY NAME(S) AND ADDRESS(ES)

Rome Laboratory/ERCP
31 Grenier St.
Hanscom AFB, MA 01731-3010

10. SPONSORING/MONITORING AGENCY REPORT NUMBER

RL-TR-96-287

11. SUPPLEMENTARY NOTES

Rome Laboratory Project Engineer: David S. Choi, ERCP, 617-377-2997

12a. DISTRIBUTION AVAILABILITY STATEMENT

Approved for Public Release; Distribution unlimited.

12b. DISTRIBUTION CODE

13. ABSTRACT *(Maximum 200 words)*

This investigation develops over-the-horizon (OTH) signal processing techniques that adaptively mitigate adverse time-varying ionospheric propagation effects. Propagation of HF radar returns through the ionosphere often results in a random spread of energy in time and space. Adaptive signal processing techniques use the statistical properties of radar clutter to measure and correct receive phase errors in an OTH radar without the need for a remote beacon. These approaches make use of complex spatial correlations between neighboring elements, or subarrays, in a phased array receive antenna to estimate and correct the differential phase errors, thereby restoring the correlation distance across the receive array to undo propagation-induced directivity and gain degradations. By compensating for time-varying spatial phase errors, this technique also reduces spread-Doppler clutter. Similarly, making use of complex temporal correlations between successive received range sweeps corrects for pulse-to-pulse errors. The algorithms are applied to OTH backscatter data collected by Rome Laboratory's VALAR facility. Results show wide variation between data sets, and as a function of range within a data set, with significant improvement in cases of severe propagation anomalies. In one instance, a combination of algorithms reduces the spread-Doppler clutter below the noise and provides 10 dB processing gain. These results imply improved subclutter visibility (SCV) in OTH radar and new methods to combat fading in long-range HF communications.

14. SUBJECT TERMS

Self Cohering, OTH Radar, Clutter, Spread-Doppler Clutter, HF Communications, Spatial Correlations, Temporal Correlation, HF Radar, Self Calibration

15. NUMBER OF PAGES

72

16. PRICE CODE

17. SECURITY CLASSIFICATION OF REPORT	18. SECURITY CLASSIFICATION OF THIS PAGE	19. SECURITY CLASSIFICATION OF ABSTRACT	20. LIMITATION OF ABSTRACT
Unclassified	Unclassified	Unclassified	Unl

ABSTRACT

This investigation develops over-the-horizon (OTH) signal processing techniques that adaptively mitigate adverse time-varying ionospheric propagation effects. Propagation of HF radar returns through the ionosphere often results in a random spread of energy in time and space. Adaptive signal processing techniques use the statistical properties of radar clutter to measure and correct receive phase errors in an OTH radar without the need for a remote beacon. These approaches make use of complex spatial correlations between neighboring elements, or subarrays, in a phased array receive antenna to estimate and correct the differential phase errors, thereby restoring the correlation distance across the receive array to undo propagation-induced directivity and gain degradations. By compensating for *time-varying* spatial phase errors, this technique also reduces spread-Doppler clutter. Similarly, making use of complex temporal correlations between successive received range sweeps corrects for pulse-to-pulse phase errors. This extends the coherent processing interval and reduces propagation-induced radar Doppler spread. The algorithms are applied to OTH backscatter data collected by Rome Laboratory's VALAR facility. Results show wide variation between data sets and as a function of range within a data set, with significant improvement in cases of severe propagation anomalies. In one instance, a combination of algorithms reduces the spread-Doppler clutter below the noise and provides 10 dB processing gain. These results imply improved subclutter visibility (SCV) in OTH radar and new methods to combat fading in long range HF communications.

i

Contents   **Page**

Figures   **Page**

Tables   **Page**

1. EXECUTIVE SUMMARY

This effort developed and experimentally demonstrated over-the-horizon (OTH) radar signal processing techniques that adaptively mitigate adverse time-varying ionospheric propagation effects such as spreading of both the receive beam and the Doppler response. Improvements in angular and Doppler resolution are necessary in order to extract weak targets from clutter. Random ionospheric disturbances and perturbations in electron density randomly spread OTH radar returns in time and space, making it difficult to coherently combine target returns received by a large aperture, over a long dwell, to obtain fine resolution in angle and Doppler, respectively. While an high frequency (HF) beacon placed within the surveillance area could be used as a reference or phase synchronizing source, the corrections derived from this beacon would only be valid in a limited region. Target returns from other locations would pass through a different part of the ionosphere and would not be properly corrected. Since land or sea clutter returns emanate from the region illuminated by the transmitter, they make ideal phase synchronizing sources. The challenge is to properly extract the required corrections from the land or sea clutter and to demonstrate the resulting improvement in OTH radar performance.

Adaptive signal processing algorithms use the statistical properties of radar clutter to measure and correct receive array phase errors in an OTH radar without the need for a remote beacon. These approaches make use of complex spatial correlations between neighboring elements or subarrays in a phased-array receive antenna to estimate and correct the differential phase errors and restore the correlation distance across the receive array, thereby compensating for propagation-induced directivity and gain degradations. To undo *time-varying* spatial phase errors, a temporal analog of this technique likewise reduces spread-Doppler clutter and Doppler spread by making use of complex temporal correlations between successive received range sweeps to correct for pulse-to-pulse phase errors. This extends the coherent processing interval and reduces the propagation-induced Doppler spread.

Various signal processing algorithms are applied to OTH backscatter data collected by Rome Laboratory's Verona-Ava Linear Array Radar (VALAR). In one instance, a combination of the spatial and temporal correlation algorithms together reduce the spread-Doppler clutter below measurable levels and provide more than 10 dB processing gain. In another case, where Doppler clutter was spread over the full unambiguous Doppler band before processing, it is confined to dc after processing. In general, the results show a wide variation between data sets, and as a function of range within a given data set. The algorithms were *not* effective when the bandwidth was decreased from 10 kHz to 5 kHz. Wider bandwidths and larger receive arrays should improve algorithm performance by providing finer resolution of the ionospheric irregularities. This would allow one to come close to recovering the error-free antenna pattern and Doppler spectrum. The potential improvement is determined by the severity of the degradation.

These results can lead to higher angular and Doppler resolution, more sensitive OTH radar systems, and to reduced site preparation for relocatable OTH radars. The temporal correlation algorithm (TCA) can improve subclutter visibility at the beamformed outputs of operational systems if I and Q data can be made available. Examination of the spatial and temporal phase corrections provides a new tool for studying long-range HF propagation. Potential applications

to HF communications include remote probing and evaluation of potential radio sites and pre-distortion of HF communication signals to combat ionospheric distortion and fading. Future work should:

(1) Further quantify, evaluate, and independently verify the results by using an over-the-horizon HF transmitter, or beacon, to simulate a target.
(2) Apply the TCA to operational OTH radar data to improve target detection and evaluate subclutter visibility improvement.
(3) Utilize wider bandwidths to increase the benefits and performance of self cohering.
(4) Apply the results to improve HF communications in the face of ionosphere-induced fades.

2. INTRODUCTION

2.1. Use and Limitations of Over-The-Horizon Radar

An over-the-horizon (OTH) radar operates in the HF band between 5 and 30 MHz, using the ionosphere to refract its waves back to the earth to provide coverage beyond the radar horizon up to ranges of 4000 km. Though antennas must be very large and spatial resolution is relatively coarse, OTH radar provides long-range and wide-area coverage at reasonable cost. Since the OTH radar effectively looks down on its targets from the ionosphere, ground or sea clutter is a critical issue that limits performance. Clutter can be reduced by improving resolution. Angular resolution may be enhanced using large antenna arrays >1 km. Range resolution may be enhanced by using a wide bandwidth waveform >10 kHz. Doppler resolution may be improved using long coherent dwells > 2 seconds. If the ionosphere acts as a perfect mirror that reflects incident HF rays, these enhancements would be easy to achieve. Unfortunately, the ionosphere is irregular and fluctuating such that:

(1) Coherence is not attained over a large receiving array.
(2) Dispersion occurs in wideband HF.
(3) Coherence is not always attained over long dwells.

In addition, the ionosphere gives rise to a phenomenon known as spread-Doppler clutter which produces clutter energy, or high Doppler sidelobes, across the entire unambiguous Doppler band [1,2]. The problems created by propagation through the irregular and fluctuating ionosphere must be solved in order to improve the sensitivity and resolution of OTH radar systems; the following defines the objective and scope of the current investigation.

2.2. Gain and Resolution Improvement by Cohering on Clutter

The primary goal is to experimentally demonstrate improved spatial and temporal coherence for a large HF receive array and a long dwell by deriving corrections from OTH clutter returns. Correcting phase errors across the aperture permits the cost effective implementation of large OTH apertures and the reduction of site preparation requirements of relocatable OTH radars. Correcting pulse-to-pulse errors reduces spread-Doppler clutter, improves signal-to-clutter ratio, and increases subclutter visibility. Both corrections increase gain and resolution: spatial coherence over a longer receive aperture increases angular resolution, while temporal coherence over a longer dwell increases Doppler resolution.

Although an HF beacon placed within the surveillance area could be used as a reference or phase synchronizing source, the corrections derived from this beacon would only be valid in a limited region. Target returns from other locations would pass through a different part of the ionosphere and would not be properly corrected. Since land or sea clutter returns emanate from the region illuminated by the transmitter, they make ideal phase synchronizing sources. The challenge is to properly extract the required corrections from the land or sea clutter and to demonstrate the resulting improvement in OTH radar performance.

The objective of this effort is to determine how well one can recover from non-ideal ionospheric propagation effects that randomly spread target and clutter energy in time and space, and to demonstrate to what extent improvement can be achieved by adaptively cohering on clutter returns. Through the use of spatial correlation and related algorithms, land/sea clutter returns are used to estimate the corrections that compensate for ionospheric propagation effects. These results are used to show that:

(1) Beam and Doppler spreading be compensated using returns from distributed clutter.
(2) Compensation can be done within the coherence time of the medium.
(3) Compensation can be done rapidly enough to reduce or eliminate spread-Doppler clutter.

This effort is an experimental investigation in which HF data, collected by the Verona-Ava Linear Array Radar (VALAR) and supplied by Rome Laboratory, is processed at GORCA to determine the extent to which clutter returns can be used to self cohere or self calibrate an OTH radar. The major tasks involve (1) the analysis and processing of three sets of existing data consisting of range-resolvable OTH radar clutter returns and (2) the specification of new data to be collected using signals from the Goosebay HF beacon along with range-resolvable clutter returns from the region that encompasses the location of this beacon.

The data processed in this effort is obtained as illustrated in Figure 2.1, where a frequency-modulated continuous-wave (FM/CW) signal transmitted from Ava is refracted by the ionosphere to illuminate a distant clutter patch on the earth from which it is backscattered and returned to the receiver at Verona via approximately the same ionosphere. Future data, using a beacon as discussed in Section 7, may be obtained as illustrated in Figure 2.2, where the beacon functions as a point source having a precisely known location. The beacon data could be processed in two ways. One, is to phase conjugate [2,3] on the beacon to derive phase corrections to be compared with the corrections obtained by cohering on the clutter. The second, is to phase steer the array to determine the angular response of the array (using the beacon as a point target) before and after self cohering on the clutter. This would provide independent verification of the gain improvements reported in Section 5.

The variation of electron density with height in the ionosphere produces multiple reflecting points that give rise to multipath and its attendant temporal dispersion. Traveling Ionospheric Disturbances (TID) and smaller-scale random perturbations in electron density give rise to refraction and scattering, respectively, producing pointing errors and spatial dispersion. Consequently, the target return will spread in time and space. The receiver aperture and receiver time gate allow us to intercept a portion of the transmitter energy scattered by the target. An "omniscient" receiver with precise knowledge of all the mechanisms of dispersion could in principle coherently recombine the received space-time samples. Since the dispersion phenomenon is random and unknown, it is necessary to determine the method of coherently combining the data from the data itself. Such a process is referred to as *adaptive beamforming* or *self cohering*. This effort addresses the extent to which clutter returns can be used to self cohere a large, digitally-beamformed OTH radar system as determined by testing and modifying various algorithms on existing and future HF backscatter radar data.
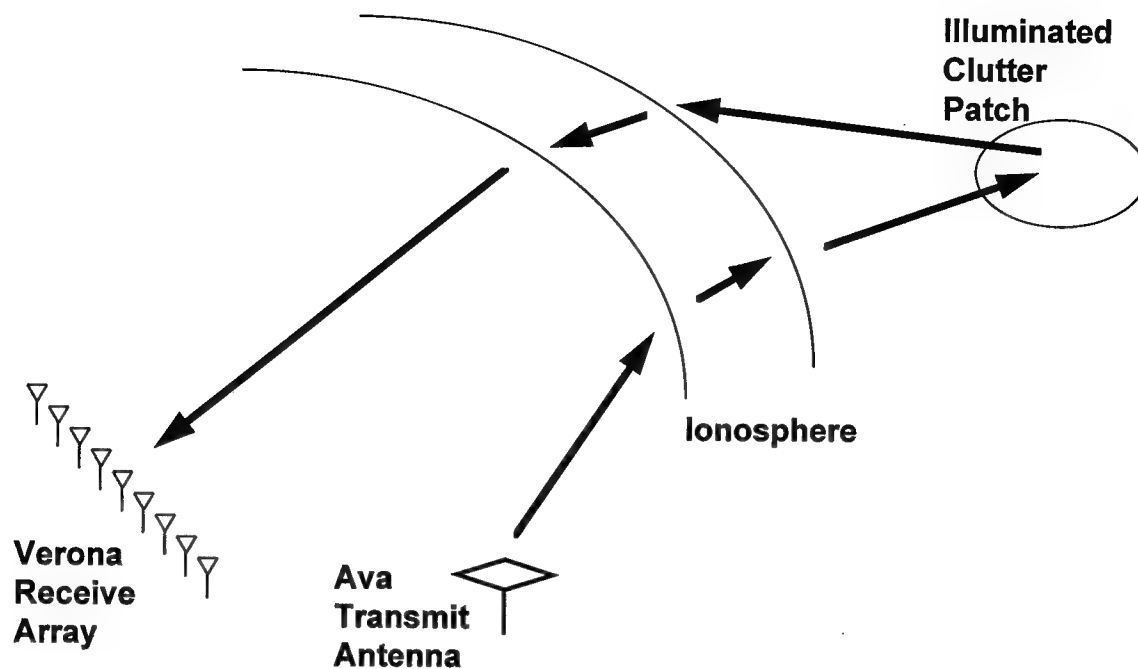
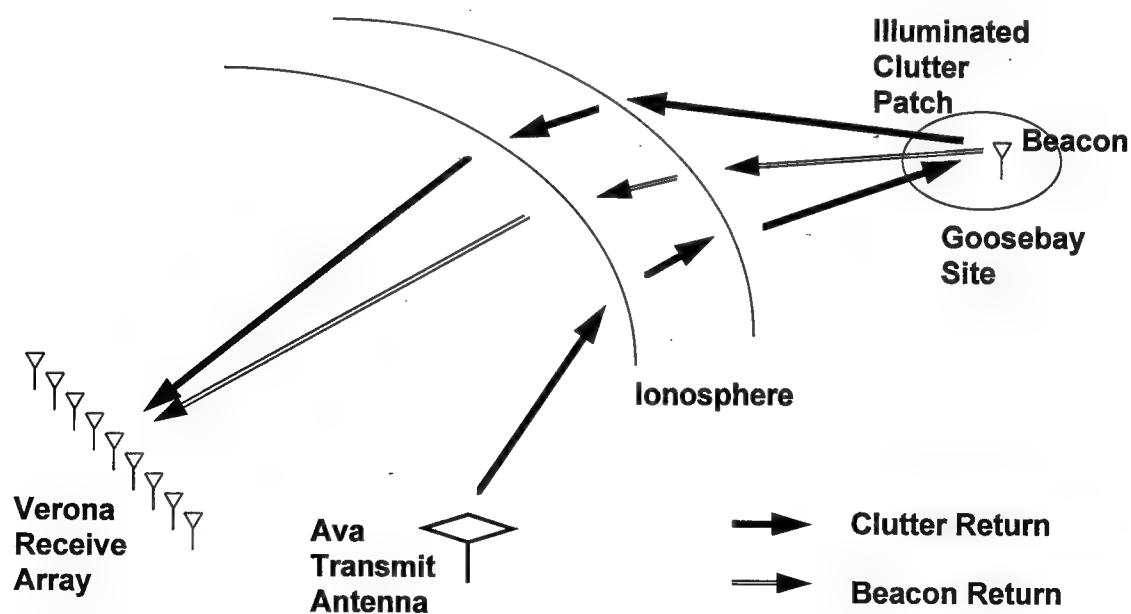Figure 2.1. Collection of OTH Clutter Returns to Cohere the Receive Array.

Figure 2.2. Collection of Beacon Data to Verify Results of Self Cohering on Clutter.

2.3. Background and Related Efforts

The effects of the ionosphere on HF electromagnetic waves has been extensively studied in [6]. An experiment for measuring instantaneous phase at eight receive sites in Philadelphia, PA due to a pulsed 9-MHz transmission from Boulder, CO is described in [7]. Use of self cohering techniques for improving the angular resolution of HF radar systems was proposed in [8]. More recently, MITRE has characterized the performance of OTH radar using analysis as well as experimental data [9,10]. Fading in long-distance HF ionospheric propagation is characterized in [11]. The spatial and temporal characteristics of auroral backscatter are described in [5]. The phenomenon of spread-Doppler clutter is characterized in [1,2]. These studies indicate that propagation through the ionosphere limits the spatial and temporal coherence of target and ground backscatter clutter returns in OTH radars. Poor spatial coherence results in broadening the mainbeam and raising the sidelobe level of both the transmit and receive apertures. Similarly, poor temporal coherence results in spreading the target and clutter energy in Doppler.

As indicated above, the signal received from a beacon, or a strong point target, could be used to compensate for the resulting spatial and temporal phase distortion through the well-established techniques of phase conjugation [12,4].[1] However, the resulting corrections would only be valid for a relatively small number of range and azimuth resolution cells surrounding the location of the point source because ionospheric effects usually exhibit strong spatial dependencies. As a result, a large number of beacons would be required throughout the area covered by the OTH radar, which is highly impractical.

The thrust of this effort is to derive the needed phase corrections based on processing the ground backscatter clutter echoes without resorting to implanted beacons or relying on finding point targets of opportunity within the scene. If successful, an OTH radar would be able to look in any direction, and, yet, recover from spatial and temporal phase errors. The Spatial Correlation Algorithm (SCA) [13-15] was the first technique that allowed self cohering on clutter returns in many phased array radar applications, including synthetic and inverse synthetic radar imagery. The SCA has also been successfully applied to laser radar, active sonar, and ultrasound. Extensions of this algorithm were developed by GORCA, including the multiple-lag SCA (MLSCA) [16,3], the phase-smoothed SCA (SSCA) [17], the iterative SCA (ISCA) [18], and the weighted least-squares SCA (WSCA) [19,20].

Other related techniques developed outside GORCA include the Shear Averaging Algorithm (SAA) [21] of Fienup, ERIM, and the Phase Gradient Autofocus (PGA) of Sandia [22]. The SAA is identical to the basic SCA, although GORCA's SCA preceded the SAA by a few years. The Phase Gradient Autofocus assumes the existence of a large number of dominant scatterers within the clutter scene. Although the PGA is known to work with some success even

---

[1]Adaptively removing spatial phase errors using phase conjugation of the signal received from a point source across the aperture is well known. Applying the same principle in the time domain to remove phase errors contaminating a sequence of pulses (or frequency sweeps) is new, especially when the temporal corrections are derived from ground backscatter returns.

if the scene is devoid of point targets, the algorithm is computationally intensive as it requires transforming back and forth between the aperture and image planes several times.

2.4. Project Methodology and Report Outline

The approach taken in this effort is both experimental and analytical. Various clutter-correlation based algorithms are used to adaptively self cohere or phase correct OTH data collected using the Verona-Ava Linear Array Radar (VALAR), an experimental HF backscatter system operated by Rome Laboratory in Verona NY. As described in Section 3, the effort requires a thorough analysis of the VALAR system and data collection in order to properly calibrate and pre-process the data prior to applying the spatial and temporal self-cohering algorithms described in Section 4. The overall project methodology is shown in Figure 2.3.

The initial approach utilizes the Spatial Correlation Algorithm to cohere VALAR data on clutter. Both single-lag and multiple-lag versions are used to correct for the phase errors across the receive array due to a non-ideal medium. If these errors are different from sweep to sweep, then sweep-by-sweep correction would reduce the amplitude of the clutter response at *non-zero* Doppler. Success consists of either (1) attaining spatial coherence over the entire 700-meter array in instances where the raw, uncorrected, received data have a shorter correlation distance, or (2) attaining full coherence over the entire 2.5-second Doppler processing dwell. Success in the first case is measured by an increase in the mainbeam and a reduction in the sidelobe level of the receive array. On the other hand, success in the second case is measured by reductions in both the Doppler spread and Doppler sidelobe level. The presently available VALAR data are used to measure the improvement in Doppler performance and future data using an HF beacon will be used to measure the array response. However, a prior indication of the potential improvement in array response is obtained by measuring the processing gain attained on zero-Doppler clutter.

It turned out that the full 10-kHz sweep was not available in the data records we were furnished. Because of transients at the saw-tooth discontinuities, only the central 200 samples of each 400-sample receive sweep were included in the data records. This effectively doubled the size of the range cell. Even when this problem was corrected as discussed in Section 3, only about five range cells could be successfully used as samples of the clutter process for self cohering. Sub-banding was not a reasonable approach under this condition because the sub-banding procedure further reduces the number of range cells used for estimating the self cohering phase corrections.

In its simplest form, the SCA initially estimates the correlation between the data received at all adjacent element or subarray pairs by multiplying the complex data samples received at each element pair, and summing this product over range. The phase of this estimated spatial correlation is used as a measure of the differential phase error from one element to the next. The element-to-element phase errors are corrected in this manner within a single sweep. By making this correction at every sweep, the time-varying errors introduced by the ionosphere are removed, and, hence, the Doppler spread and the Doppler sidelobes are reduced. The latter Temporal Cor-

7

Section 3

VALAR Data Collection

Model VALAR System

Calibraiton and Correction of VALAR Data

Section 4

Self-Cohering Data Processing

Section 5

Spatial Correlation Adaptive Processing

Evaluation of Results

Temporal Correlation Adaptive Processing

Evaluation of Results

Hybrid Spatial and Temporal Correlation Processing

Sections 5 & 6

Evaluation of Results

Section 7

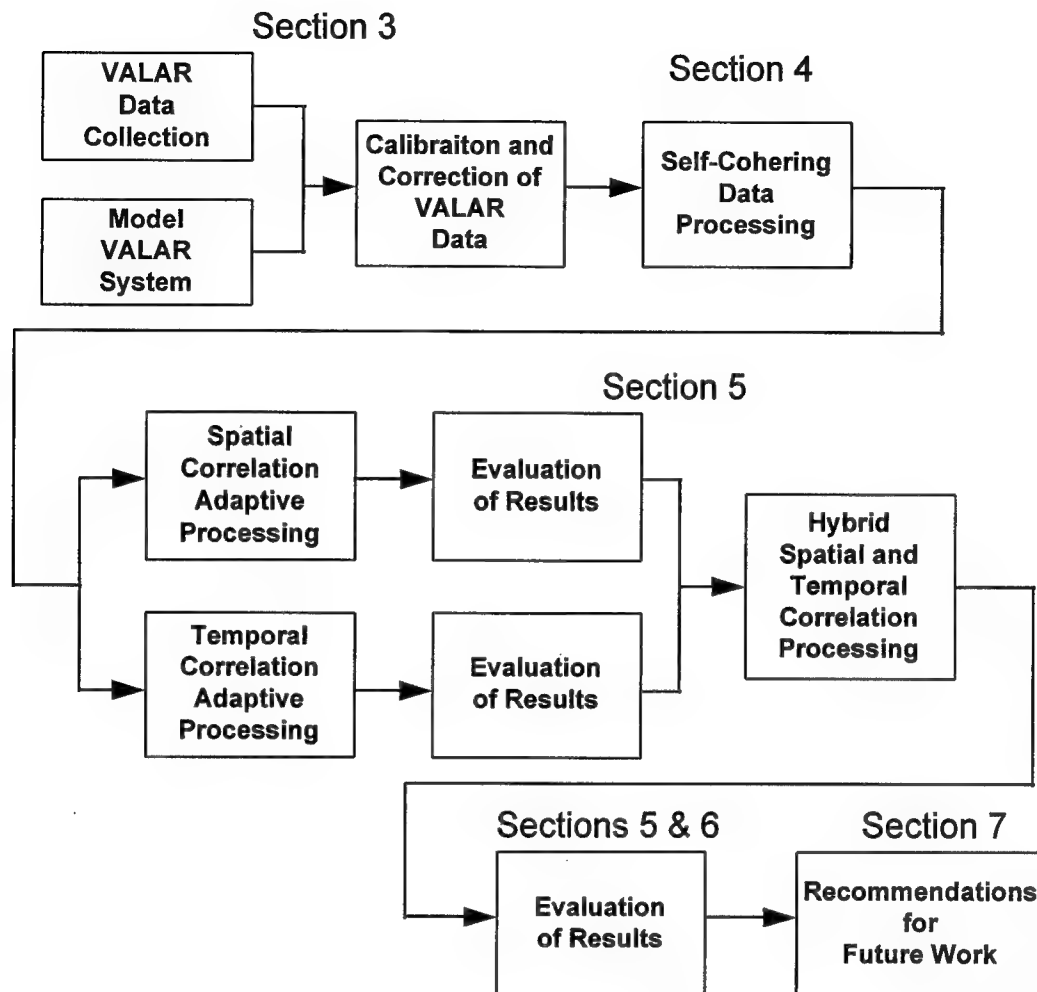Recommendations for Future Work

Figure 2.3. Project Methodology.

8

relation Algorithm is a recent GORCA invention developed to compensate for temporal phase distortion due to ionospheric effects. By combining the SCA and TCA we remove both element-to-element and sweep-to-sweep phase errors.

For the SCA, averaging over sweeps may be performed to increase the clutter-to-noise ratio before multiplying the returns for self cohering. This corresponds to first doing Doppler processing at the element level and then applying the SCA to the zero-Doppler data. For the TCA, averaging over elements can be done before processing data from adjacent sweeps. This corresponds to first beamforming and then applying the TCA to the beamformed output because the data at the element level is too noisy for the TCA to produce useful results. When this is done, the beamforming is best done after applying the SCA.

The number of range cells used to estimate the correlation must be large enough to provide a good estimate, but small enough so that the quantity being estimated remains relatively constant over the range interval used. The number of sweeps averaged before using the SCA must be large enough to increase the clutter-to-noise ratio, but it must be smaller than the coherence time of the medium. Thus, temporal coherence can be improved slightly by applying the TCA at the element level. The number of elements averaged before final application of the TCA must be large, but it must not exceed the spatial coherence of the received data. By applying the SCA first, we found that all 36 elements could be used in this step.

We, thus, see that there are a large number of processing alternatives. In every case the parameters and procedures are varied to maximize the peak processed clutter return at zero Doppler. An additional variable is the specific algorithm used. The previous discussion assumes that the simple single-lag Spatial or Temporal Correlation Algorithm, in which only a single spatial or temporal nearest neighbor, is used. Other algorithms include: (1) smoothed versions, (2) iterative versions, and (3) multiple-lag correlation algorithms. The multiple-lag algorithms vary in the number of lags utilized and in the manner in which the redundant, over-determined, phase-error measurements are statistically combined to arrive at phase corrections. The optimal algorithm is presented in Sections 5.1 and 5.2, the results obtained after optimizing are presented and evaluated in the remainder of Section 5, and conclusions are drawn in Section 6. The specification of beacon requirements for use in further verification and evaluation of the results is given in Section 7.1 as part of the recommendations for future work.

9

3. VALAR SYSTEM AND DATA DESCRIPTION

In the following, we first discuss the VALAR system. Afterwards, we discuss the data collected and describe the manner in which these data were processed and present the results. By reviewing the VALAR system and waveform we were able to identify and correct factors that limited its performance. As described below, we (1) enhanced the range resolution by 90% in order to correctly estimate the required phase corrections and (2) calibrated the array from sweep to sweep (pre-Doppler) in order to eliminate any Doppler spread that might be present due to system instabilities.

3.1. System Description

The Verona-Ava Linear Array Radar (VALAR) is schematically illustrated in Figures 3.1 and 3.2 and the system parameters are given in Table 3.1. The 300 kW rhombic FM/CW transmitter in Ava, NY produces a 10 kHz bandwidth signal anywhere between 3 and 12 MHz. The receiver in Verona, NY is a 700-meter linear array of 36 quadrapole elements spaced 20 meters apart. Broadside is 10 degrees east of true north. This array has separate I and Q receivers at each of the 36 elements. Data is taken looking north with a 2.5-second, 64-pulse, coherent dwell. Prior to analyzing and processing the November data files, an examination of the OTH radar system and waveform was made to determine whether system parameters and system errors were limiting the performance of the self cohering algorithms. The transmitted waveform and the corresponding receiver processing are illustrated in Figures 3.3 and 3.4.

Figure 3.1. The VALAR System.
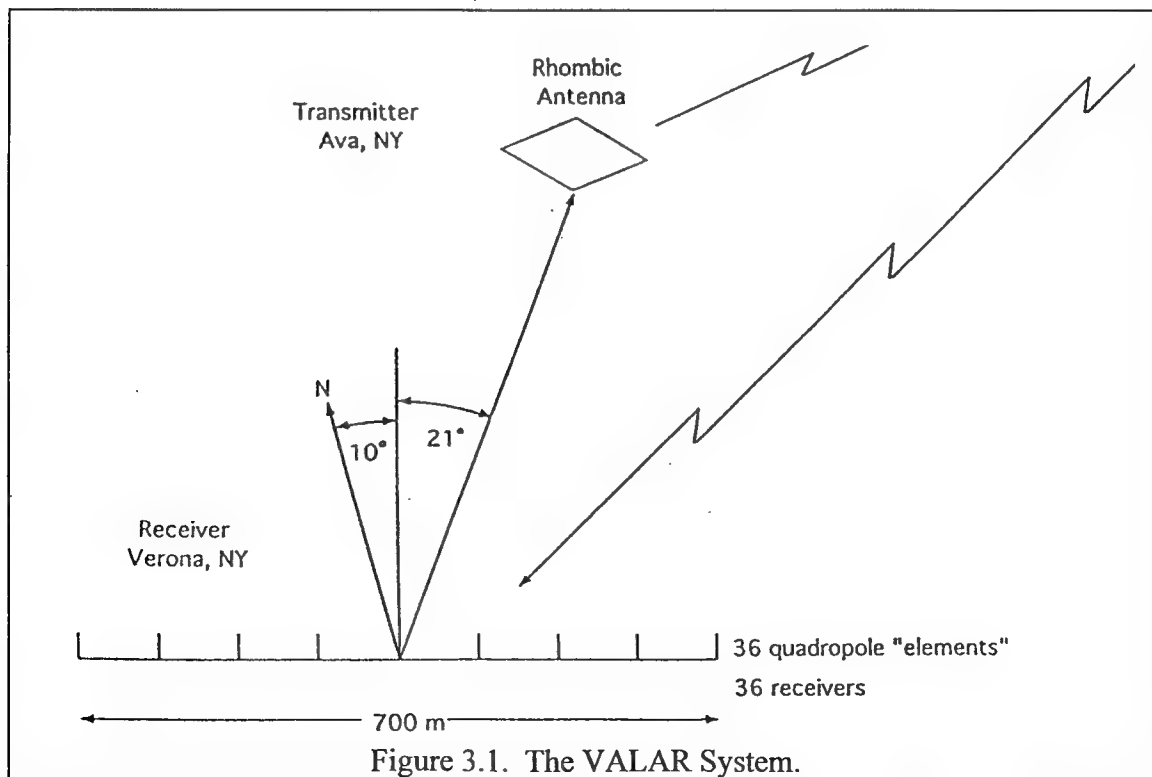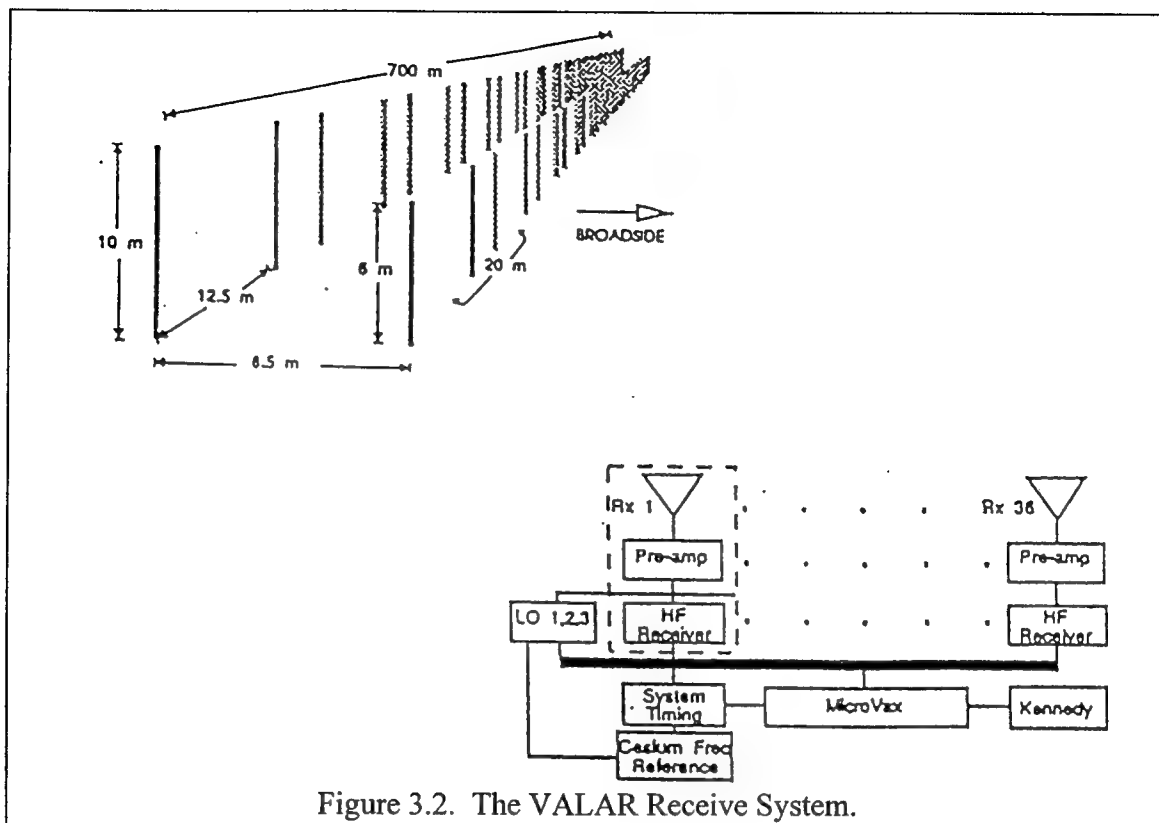
Figure 3.2. The VALAR Receive System.

Table 3.1. VALAR System Parameters

	Transmitter	Receiver
Location	Ava, NY	Verona, NY
Operating Frequency	3 - 12 MHz	
Power	100 kW, CW (max 300)	
Antenna	Rhombic	700 m array of 36 quadrapoles
gain	21 dB (estimated)	23 dB
az. beamwidth	14 deg	3 deg
el. beamwidth	14 deg	42 deg (calculated)
az. sidelobe level	14 dB	30 dB rms
Instantaneous Bandwidth	10 kHz	
Waveform	10 kHz sweep in 1,000 steps	
WRF	25 sweeps/sec	
Dwell	2.5-3.2 sec. (64-81 sweeps)	
LO frequency offset	5 Hz	5 kHz
Phase at end of LO sweep	zero (due to 5 Hz offset)	0.2 cycles (72 deg)
A/D sampling rate		10,000 samples/sec, I and Q (400 samples/sweep)

11

Figure 3.3. Transmitted Waveform.

Figure 3.4. Receiver Waveform Processing.
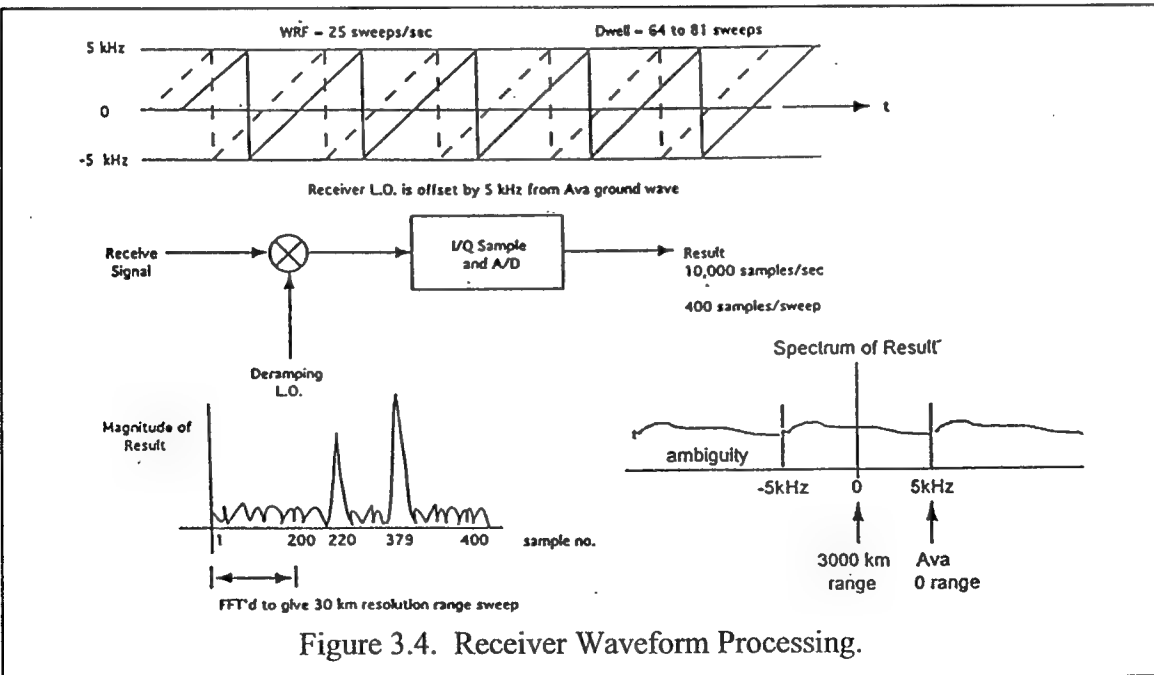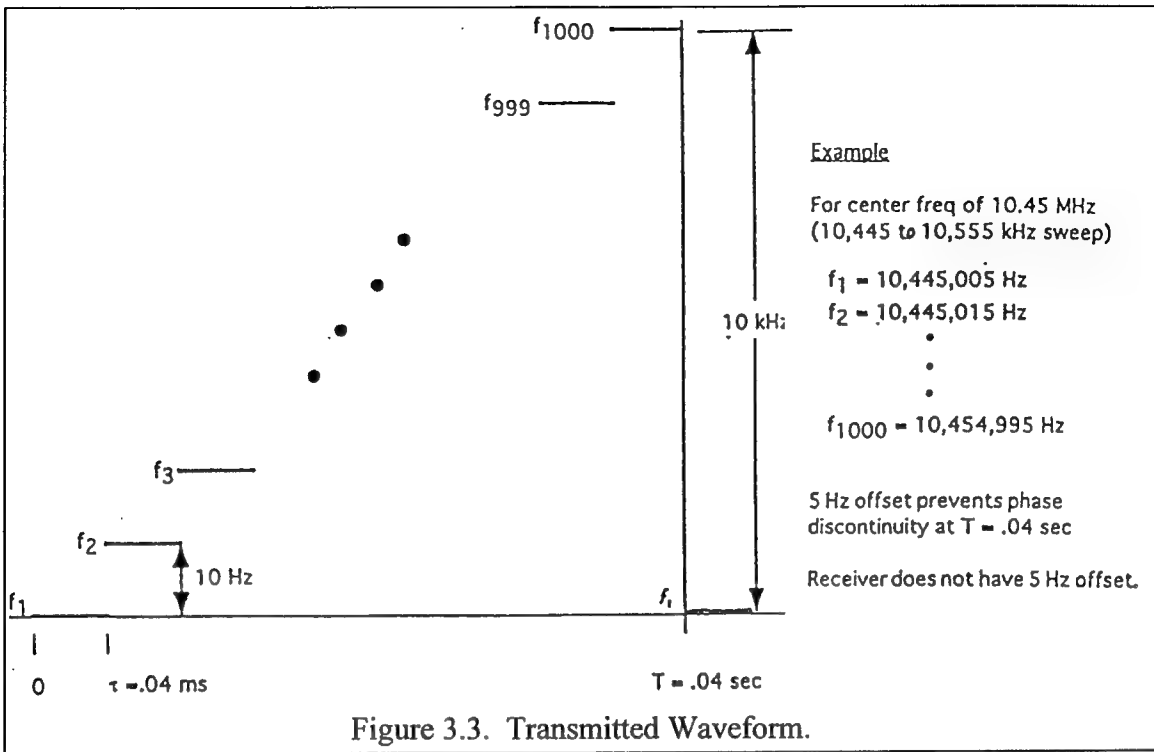
Note that the receiver local oscillator (LO) is offset by 5 kHz so that the zero range bin is at 5 kHz after the deramped result is FFT'd. The transmitted frequencies are as listed at the right of Figure 3.3 so that a full number of cycles occur during a waveform repetition period (i.e., the

12

phase returns to zero). If the sequence 10,445,000, 10,445,010, ... were used, a $2\pi/5$ phase discontinuity would occur at the end of each sweep.

3.2. Range Resolution Enhancement

Figure 3.5 shows a typical deramped sweep in the Nov01504 data set at each of the 36 elements. Amplitude "glitches" occur at Sample Nos. 219/220 and 379/380 as seen in the amplitude plot of Figure 3.6. These glitches are due to the 5 kHz offset between the receiver LO and the received Ava groundwave waveforms which produces discontinuities at these locations as shown in Figure 3.7.

(a)   (b)

Figure 3.5. Single Sweep for All 36 Elements. (a) Raw Data. (b) After Post-Doppler Calibration

Figure 3.6. Typical Raw Amplitude Sweep.

Figure 3.7. Origin of Glitches.

13
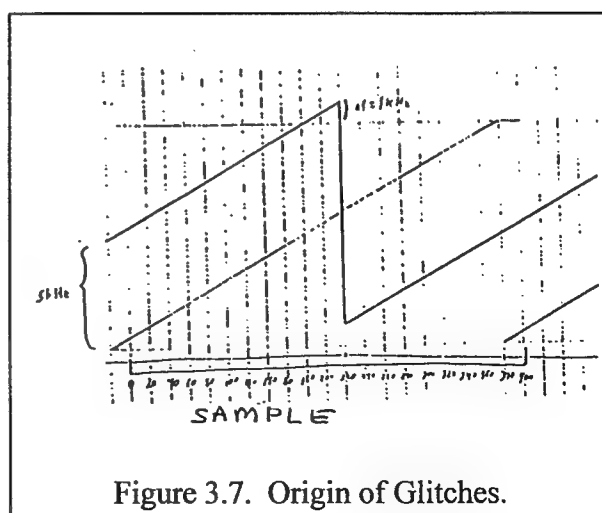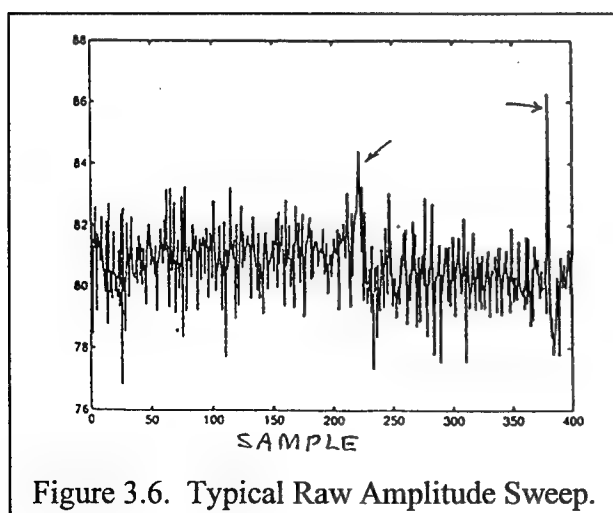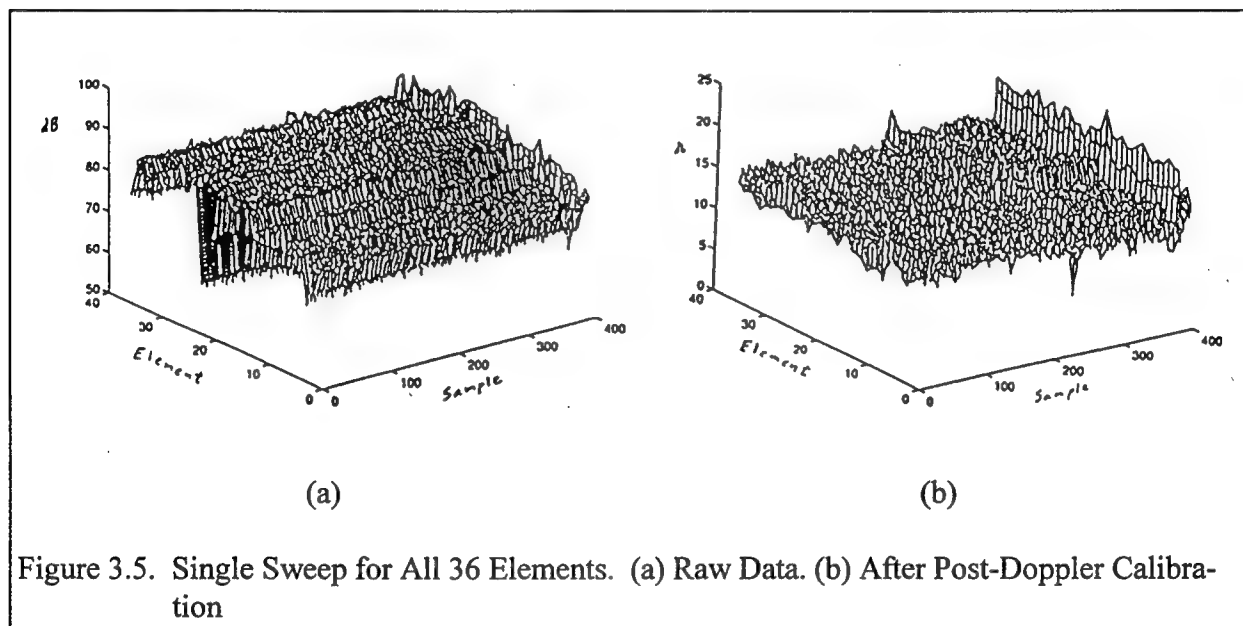
At first, the glitches caused us to use only 200 of the 400 samples as input to the range FFT, resulting in 30-km range resolution. Self cohering determines phase corrections from cross-correlations that are estimated by averaging products over many range bins. The number of range bins that can be used is severely limited by the elevation scale size of the ionospheric irregularities. Range resolution finer than 30 km is essential if self cohering is to be successful. Attempts were made to correct the glitches by linear filtering, but filtering out the 5-kHz line corresponding to the Ava groundwave range cell made the glitches even larger, regardless of the type of filter used; a nonlinear response caused by a signal discontinuity cannot be corrected by linear filtering. Referring to Figure 3.8, which shows the phases of four typical raw data sweeps, similar to the amplitude sweep shown in Figure 3.6, a phase transient occurs at Sample Nos. 219/220, corresponding to the Ava groundwave frequency jump. On the other hand, both a phase transient and a phase step occur at Sample Nos. 379/380, corresponding to a combined local oscillator frequency jump *and* $2\pi/5$ phase jump. This led to the nonlinear correction scheme described in Section 4.3. The net result was the recapture of 378 samples, instead of 200, in the range FFT, improving the range resolution by about 90% from 30 km to 16 km.

Figure 3.8. Phases of Typical Sweeps.
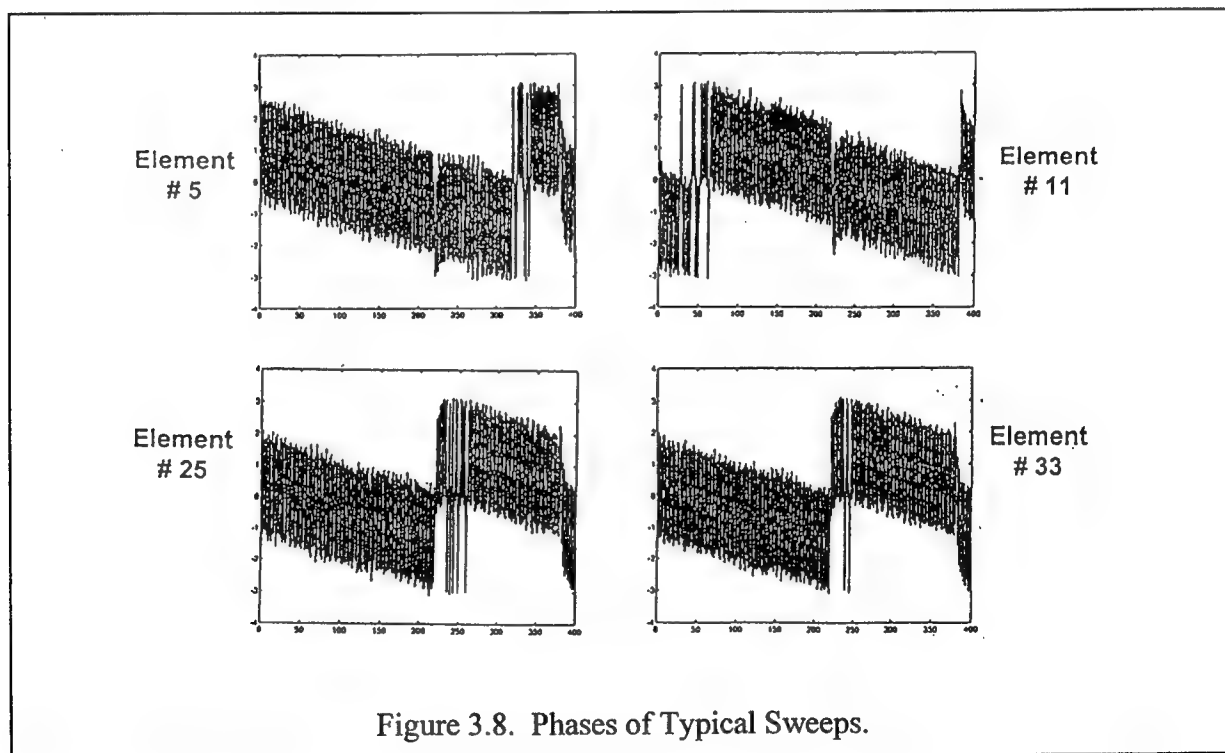
3.3. Pre-Doppler Array Calibration

The Ava groundwave has been used to correct for element-to-element amplitude and phase errors due to the system (as opposed to the ionosphere). This has no effect on sweep-to-sweep system phase errors (e.g., due to oscillator phase instability) that can raise the near-in Doppler sidelobes. Figures 3.9 and 3.10 show the range response at a typical element before and
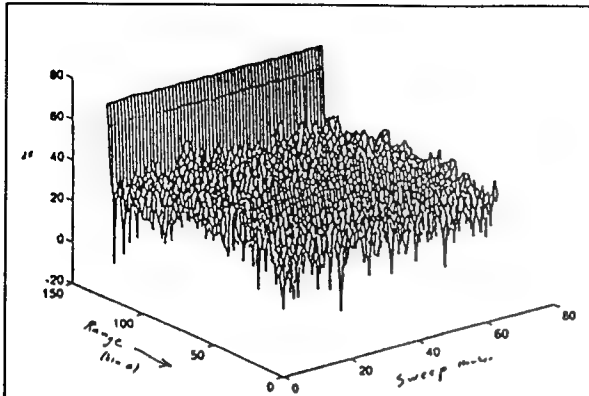
Figure 3.9. Single Element Range Sweeps.
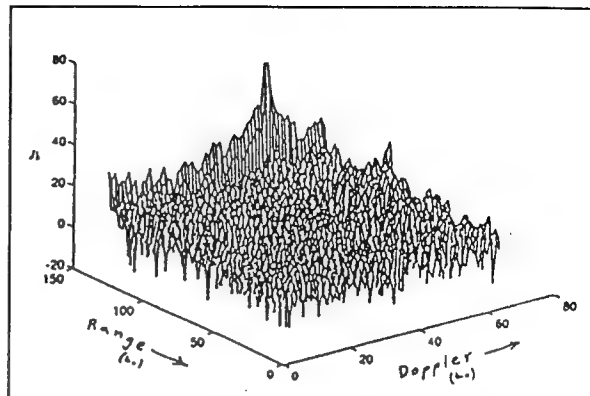
Figure 3.10. Single Element Range-Doppler
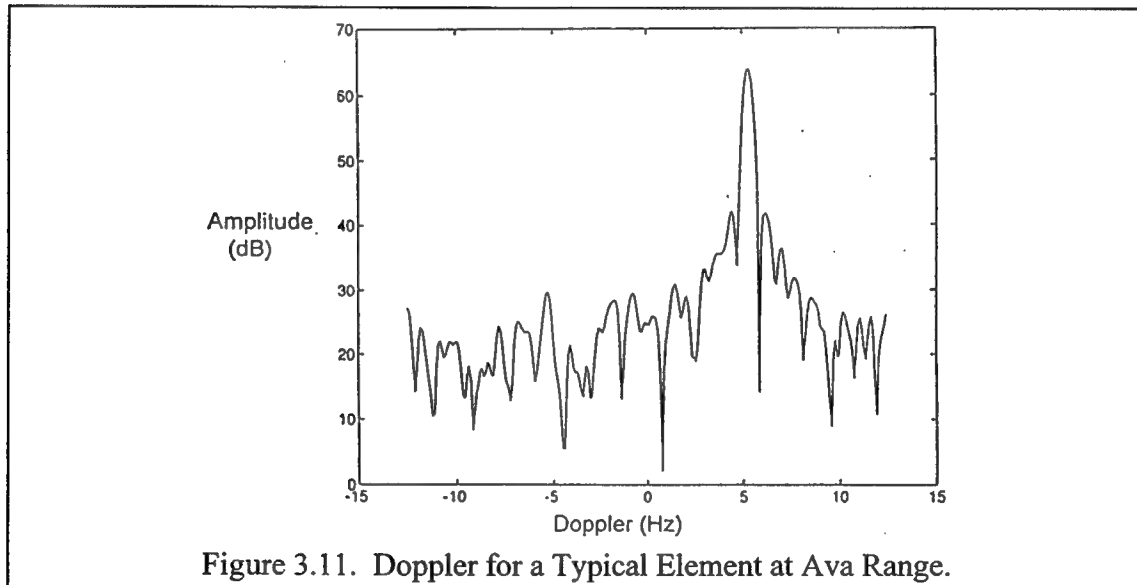
Figure 3.11. Doppler for a Typical Element at Ava Range.

after performing the Doppler FFT. As can be seen from the range response to Ava (bin 128), the range response of the system is excellent. As can be seen from the Doppler response at the Ava range bin (Figures 3.10 and 3.11), the Doppler response of the system exhibits high near-in sidelobes.

The standard calibration file supplied to GORCA was a 36-element complex vector obtained from the Ava groundwave after performing a two-dimensional, range-Doppler FFT. As seen in Figure 3.12, this corrects for element-to-element errors without affecting the Doppler response. To improve the Doppler response we correct for sweep-to-sweep errors, as well as element-to-element errors, by creating a new calibration file consisting of a 36 by 81 complex matrix obtained from the Ava range bin after performing only a one-dimensional (range) FFT. The

number of columns in the new calibration file is equal to the number of sweeps (81 for Nov01054 and 80 for Nov01056). The improved single element result, corresponding to Figure 3.10, is shown in Figure 3.13. The Doppler response to Ava (bin 128) is an ideal Hamming weighted response; the 64-point Doppler FFT used in Figure 3.13 shows its envelope only.

nov01504 uncalibrated   nov01506 uncalibrated

nov01504 with post-Doppler calibration

Post-Doppler Calibration does not reduce the high near-in Doppler sidelobes

Figure 3.12. Doppler at Each Element for Ava Range Cell.

Figure 3.13. Single-Element Range-Doppler After Pre-Doppler Calibration
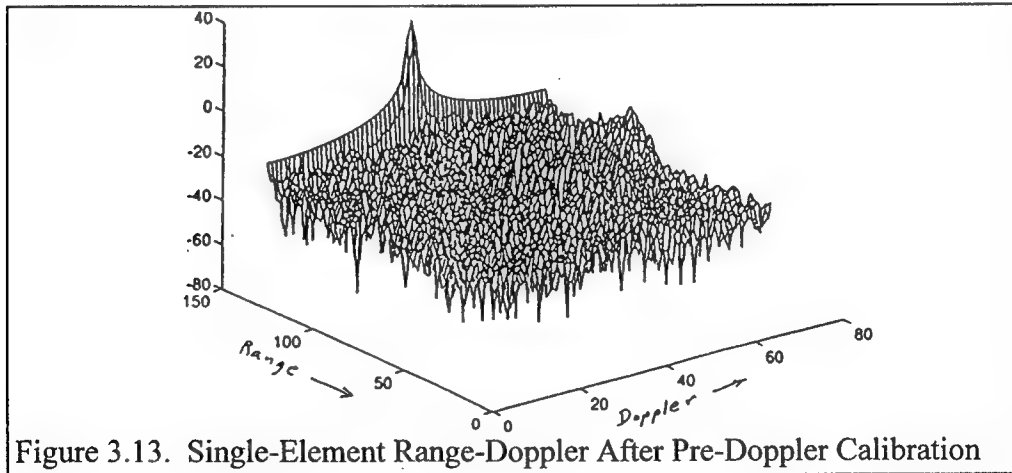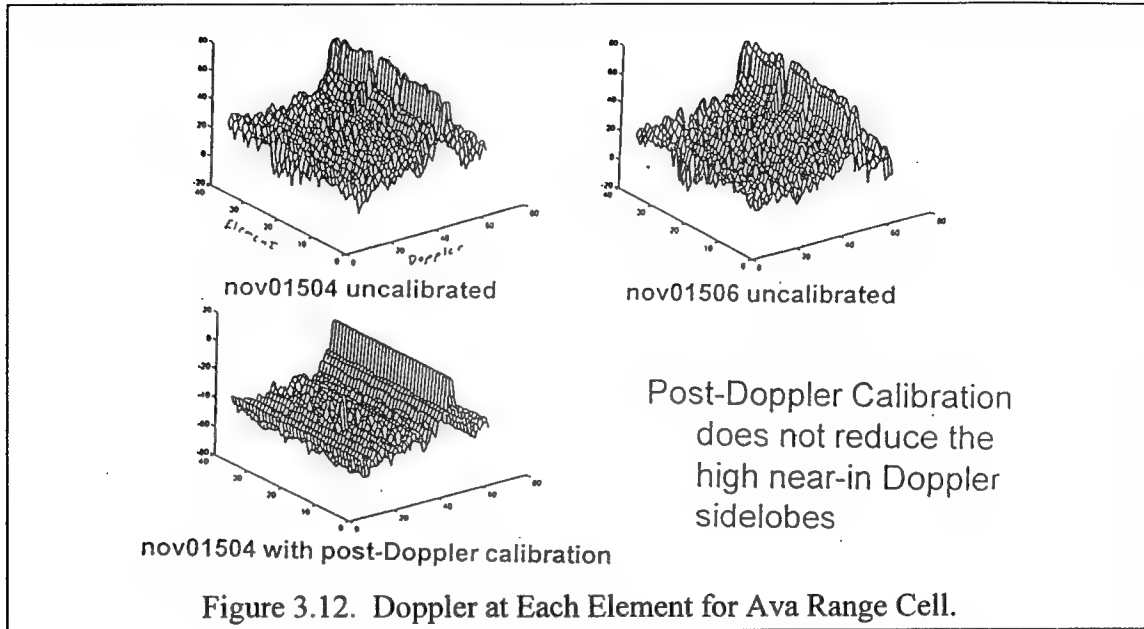
The final results for post-Doppler versus sweep-to-sweep pre-Doppler calibration, after beamforming, but before self cohering on clutter returns, are given in Figures 3.14 through 3.16. In Figure 3.14, the significant improvement in the Doppler response at the Ava range bin is preserved in the beamforming process. In Figures 3.15 and 3.16, the Doppler improvements at other range bins in the amplitude-range-Doppler (ARD) map are minor. This is a strong indication that the Doppler spread and Doppler sidelobes are *not* primarily due to transmitter phase instabilities.

Post-Doppler Ava Calibration | Pre-Doppler Ava Calibration

Figure 3.14. Range-Doppler Plots for Peak Beam.

Figure 3.15. ARD Post-Doppler Calibration.

Figure 3.16. ARD Pre-Doppler Calibration.

17
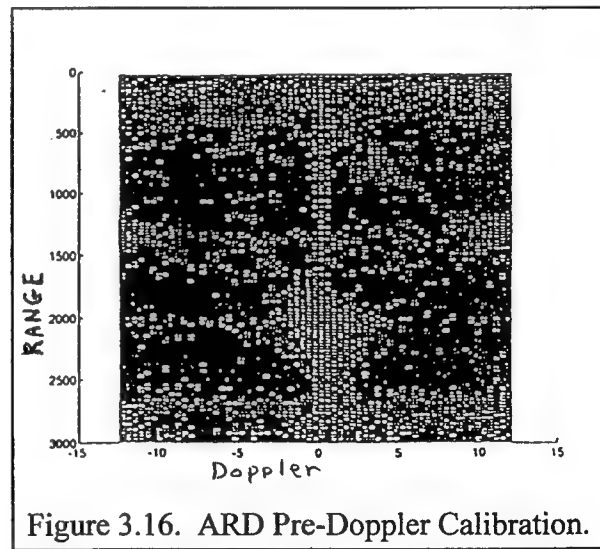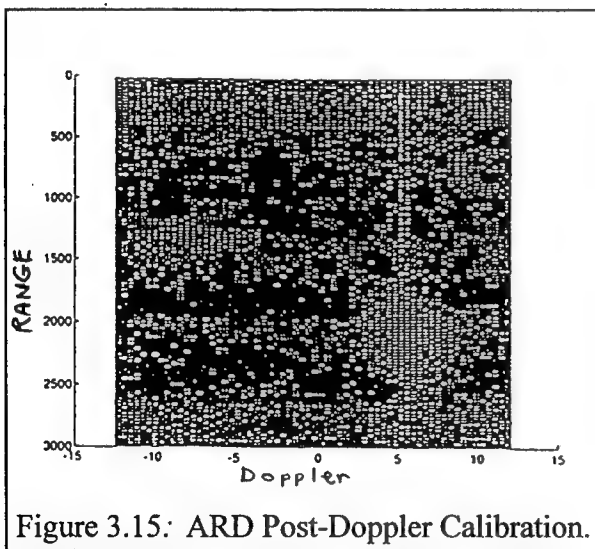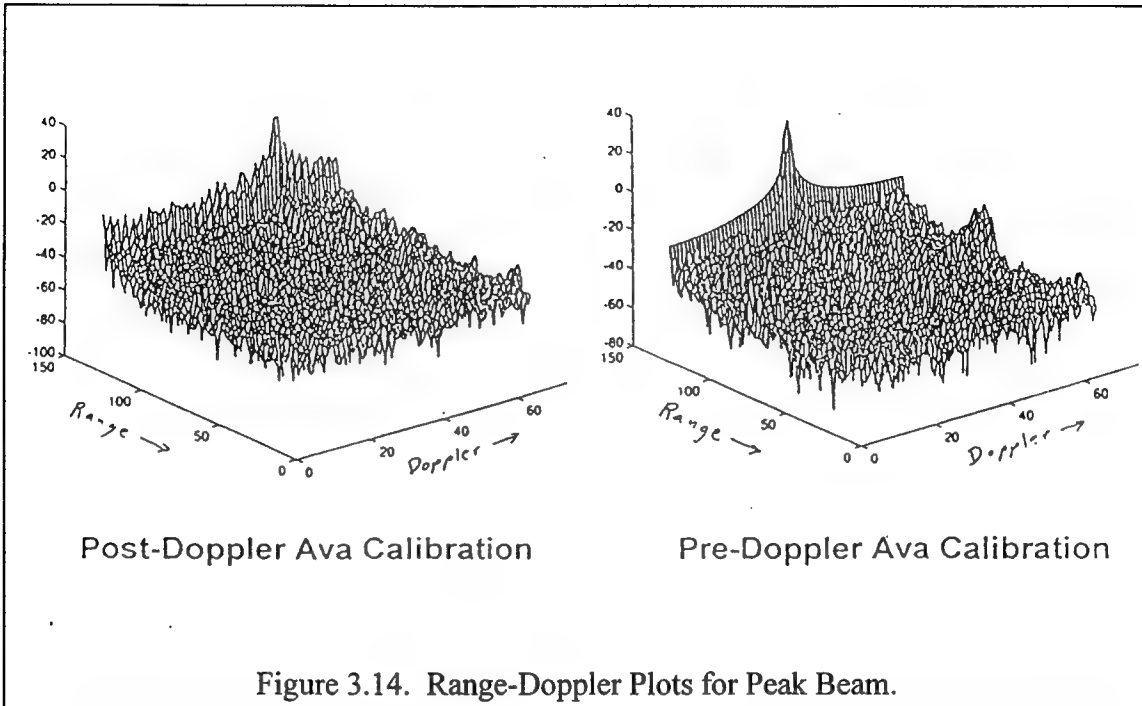
4. SELF COHERING ALGORITHMS

The objective of this effort is to experimentally show that it is possible to improve the spatial and temporal coherence of OTH radars by using ground backscatter returns without resorting to implanted beacons or relying on finding point targets of opportunity within the clutter scene. This would enable an OTH radar to freely look in any direction, and, yet, recover from spatial and temporal phase distortion caused by propagation through the ionosphere. Table 4.1 gives a comprehensive list of data-adaptive, phase-compensation techniques. We also refer to these algorithms as "self cohering" or "autofocusing" techniques.

<u>Table 4.1. Self Cohering/Autofocusing Techniques</u>

• Dominant Scatterers Based Algorithms
  - Dominant Scatterer Algorithm (DSA): Steinberg (Univ. of Pennsylvania) [12]
  - Multiple Scatterer Algorithm (MSA): Attia (GORCA) [23-25]
  - Phase Gradient Autofocus (PGA): Eichel, Ghiglia, and Jakowatz (Sandia) [22]
 	
• Spatial Correlation Based Algorithms
  - Spatial Correlation Algorithm (SCA): Attia (GORCA) [13-15]
  - Multiple Lag Least Squares SCA (MLSCA): Subbaram/Attia (GORCA) [16,3]
  - Weighted Least Squares Multiple Lag SCA (WSCA): Attia/Abend (GORCA) [19,20]
  - Phase Smoothed SCA (SSCA): Stockburger/Abend (GORCA) [17]
  - Iterative SCA (ISCA): Attia (GORCA) [18]
  - Shear Averaging: Fienup (ERIM) [21]
 	
• Energy Constraint Method: Tsao/Subbaram (GORCA) [26,27,3]
 	
• Image Plane Differential Phase Smoothing: Kupiec (MITLL)

Because trying to find strong targets of opportunity would be unreliable, dominant scatterers-based algorithms are excluded. Although it was reported in [22] that the PGA had some success with autofocusing scenes that lacked dominant scatterers, this algorithm is computationally intensive and fails in the presence of large or uncorrelated phase errors. We also exclude the Energy Constraint Method [26,27,3] because of its computational complexity and lack of good experimental results. We focus our attention on spatial correlation-based algorithms because they are robust, computationally efficient, perform well in the presence of large phase errors, and do not require targets of opportunity. In the remainder of this section, we describe (1) the basic Spatial Correlation Algorithm, (2) the subarray processing method utilized with the VALAR data, and (3) an improved phase-unwrapping method used to ascertain the beampointing direction after self cohering.

18

4.1. The Spatial Correlation Algorithm

The Spatial Correlation Algorithm [13-15] enables self cohering of distorted arrays in the absence of dominant scatterers, or targets of opportunity, using the spatial correlation properties of radar clutter. Array distortion can be either geometrical due to lack of accurate knowledge of element positions, as would be the case for a non-motion-compensated SAR, or electrical due to different cable lengths, mismatches, etc. Moreover, distortion of the phase front due to propagation anomalies can often be modeled as a pattern of phase errors across the array, and, hence, can be compensated. The array itself is assumed to be fairly general. It can be random or periodic, physical or synthetic, transmit/receive or receive only. The main restriction is that the *inter-element* spacing should not exceed the spatial-correlation distance of the clutter returns which is roughly equal to half the size of the transmitting aperture [13]. This restriction is easily met in many applications. It is certainly met in the Ava-Verona HF backscatter system, where the size of the transmit aperture is about four times the inter-element spacing of the receive array.

Let us consider a bistatic system with a relatively small well-formed transmit aperture and a large distorted receive array. Before forming the receive beams, the phased array has to be cohered; i.e., phase errors across it due to ionospheric effects must be removed. Let us assume for the moment that the transmitter is pointing at array broadside. The algorithm relies on measuring the nearest-neighbor spatial correlation between clutter signals received by the array elements over range. The basic idea behind the algorithm is that $R(X)$, the spatial correlation function of clutter returns at the aperture, will be *real* provided the clutter illuminated by the main-beam of the transmitter is statistically homogeneous when averaged over range.[2] Non-zero arguments of the measured correlations are attributed to phase errors at the array elements. We will show that these array phase errors can be estimated from the correlation measurements, and, hence, can be compensated for.

To illustrate, let us consider the simple case of a linear, periodic receive array with inter-element spacing d. In the absence of phase errors in the array, each pair of adjacent elements, forming an interferometer of size d, should measure the *same* quantity $R(d)$ irrespective of its position along the array. This is a direct consequence of the assumed spatial stationarity of the random process representing clutter returns across the aperture. Further, if $R(d)$ is real, then each element pair will be measuring $|R(d)|e^{j0}$. However, in the presence of a phase error pattern given by $\{\delta_n | n = 1,...,N\}$ across the N-element receive array, correlation measurements will reflect these phase errors. In particular, the *n-th* correlator formed by elements number n and $n+1$ will be measuring $|R(d)|e^{j[\delta_n - \delta_{n+1}]}$. That is, the argument of the correlation measurement made by each element pair gives a direct estimate of the difference between the two phase errors suffered by the pair of elements involved. We will show that the available *N-1* phase difference estimates are sufficient to estimate the phase-error pattern across the aperture within an unknown but unimportant additive constant phase term. This estimated phase-error pattern can be used to focus the array by subtracting it from the phases of the received data across the aperture. Then, the receive beams can be digitally formed by Fourier transforming the corrected data. It is important

---

[2]X is the spatial lag along the receive aperture, or the length of the interferometric baseline over which the spatial correlation of ground backscatter is being measured.

to note that the SCA places no restrictions on the range of initial phase errors it can correct for. Since the solution is direct and non-iterative, initial phase errors can range anywhere between $-\pi$ and $+\pi$, and can be independent from one spatial sampling position to the next without affecting the performance of the algorithm.

Let us assume that the field measured at the *n-th* array element is given by $e'_n = e_n e^{j\delta_n}$, where e_n is the error-free value produced by a large number of non-coherent scatterers within the illuminated clutter patch, and δ_n is the phase error due to propagation anomalies. The *n-th* correlator provides an estimate, $\hat{R}'_n$ of the quantity

$$
\begin{aligned}
R'_n &= E\{e'_n e'^*_{n+1}\} = E\{e_n e^*_{n+1}\}e^{j(\delta_n - \delta_{n+1})} \\
&= R(d)e^{j(\delta_n - \delta_{n+1})}.
\end{aligned}
\tag{4.1}
$$

Since $\hat{R}'_n$ is estimated over range, we compute for M range cells

$$
\hat{R}'_n = \frac{1}{M}\sum_{i=1}^{M} e'_n e'^*_{n+1} ,
\tag{4.2}
$$

where i denotes the *i-th* range bin. The phase of $\hat{R}'_n$, denoted by ψ_n, is the quantity of interest. Assuming that we have good phase estimates $\{\psi_n\}$, we can approximate these by

$$
\psi_n \approx (\delta_n - \delta_{n+1}) + \beta_n \qquad n = 1, \cdots, N-1,
\tag{4.3}
$$

where $\beta = \arg\{R(d)\}$. Next, we form the quantity

$$
\phi_n \equiv \sum_{k=1}^{n-1} \psi_k
\tag{4.4}
$$

$$
\approx (\delta_1 - \delta_n) + (n-1)\beta ,
\tag{4.5}
$$

which we use as a phase correction by adding it at the *n-th* array element, for all n. The total phase shift becomes

$$
\delta\phi_n = \delta_n + \phi_n
\tag{4.6}
$$

$$
\approx \delta_1 + (n-1)\beta
\tag{4.7}
$$

The phase $\beta(X)$ of the spatial correlation function plays a major role in cohering the array. If the spatial correlation function is real and positive in the region of interest then $\beta = 0$, and we have an ideal situation for which Eq (4.7) reduces to

$$
\delta\phi_n \approx \delta_1 = constant\ inependent\ of\ n ,
\tag{4.8}
$$

and the random variables δ_n are replaced by a constant. The result is a well-focused aperture.

The assumption that the spatial correlation function at the receive aperture $R(X)$ should be real is a direct consequence of the Fourier transform relationship that exists between the clutter illumination intensity function $I(u)$ and $R(X)$ [13]. $I(u)$ describes the average power reradiated by the scattering centers within the illuminated sector as a function of the reduced angular variable u. If the clutter is statistically homogeneous over range, $I(u)$ will be proportional to the power pattern of the transmitter $|f(u)|^2$, which is real by definition. A real symmetric $I(u)$ will result in a real $R(X)$. From the symmetry of the problem it is evident that the beam so formed will point in the direction of the axis of symmetry of the transmit antenna. It is worthwhile to note that the Fourier transform relationship that exists between $R(X)$ and $I(u)$ in the space-angle domains, namely the van Cittert-Zernike theorem, is analogous to the Wiener-Khintchine theorem that relates the temporal autocorrelation function $R(\tau)$ and the power spectral density $S(f)$ of a temporal random process in the time-frequency domains.

As prescribed by Eq (4.2), we can estimate the required correlations by averaging the correlation readings, or cross-products, based on the echoes originating from successive range cells, provided that the geometrical features of the scatterers are statistically homogeneous over the area of interest.[3] To insure the statistical homogeneity of the scatterers, we can estimate the correlation values over a large number of range bins. This will tend to decorrelate the large-scale features of the scattering centers.

At this point, let us remove the assumption of broadside illumination. Far-field clutter returns due to a transmit beam making an angle θ_o with the array broadside will result in a linear phase progression across the receive aperture. This linear phase term, proportional to $\sin\theta_o$, can be lumped into the quantity δ_n representing the phase error at the n-th element in the above equations. Because the SCA enables us to estimate and remove $\{\delta_n\}$, the resulting receive beam will be retrodirective in the sense that it will follow the axis of symmetry of the transmit aperture all the time.

The Spatial Correlation Algorithm is a very robust self cohering, or autofocusing, technique. Although independence of the clutter scene can be forced by estimating the correlation values over a large number of range bins to insure the statistical homogeneity of the scatterers, the algorithm does not degrade rapidly as the number of range bins decreases. As few as 5 range bins have been found to be adequate [17]. Even if $R(X)$ were complex, with $\beta \neq 0$, it would still be possible to self cohere the aperture. A small beam-pointing error proportional to the slope of the phase of $R(d)$ will result in this case, however. This can easily be seen from Eq (4.7) where the linear phase term $(n-1)\beta$ will cause the squint. Finally, we note that the Shear Averaging Algorithm (SAA) [21] of Fienup, ERIM, is identical to the basic SCA.

---

[3]This amounts to assuming ergodicity of the random process representing ground clutter.

4.2. Subarray Processing

In our initial work, spatial corrections were based on correlating clutter returns from one array element to the next. Because the transmit beam illuminates a fairly wide angle, the corrections pertain to the direction of the centroid of the intensity distribution of the illuminated clutter, which is often, but not always, given by the direction of the peak of the transmitter pattern. These corrections are not valid for other receive look directions. To alleviate this problem, some directivity to the phase corrections is introduced by dividing the 36-element array into a number of overlapping subarrays and computing the phase corrections for a particular look direction by correlating the outputs of adjacent subarrays after steering each subarray to the desired azimuth. Element-to-element corrections are obtained by linear interpolation/extrapolation between the phase centers of the subarrays. The algorithm we implemented performs two iterations for subarray sizes of 12 and 18 elements, where 50% overlap between consecutive subarrays is maintained. For the Nov01504 data, this results in a shift from the original beam position b to a new position $b' = b + 2.6$ degrees azimuth, for each beam.

Figure 4.1. (a) Original 2π-Ambiguous Phase Corrections. (b) Unwrapped Phase Corrections.
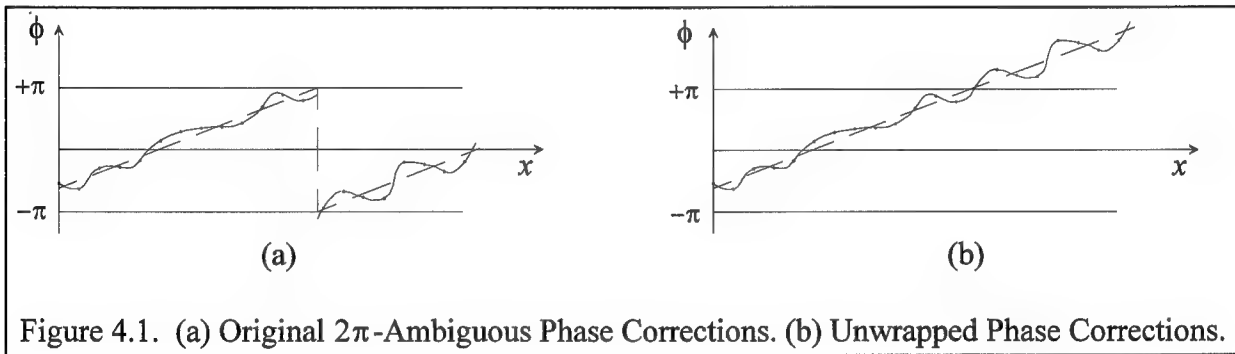
4.3. Phase Unwrapping

Spatial corrections applied to the receive array data make the array *retrodirective* in the sense that the center of illumination is shifted to array broadside in an azimuth-range map. To determine the absolute azimuth position in such a map, we need to estimate the amount of azimuth shift resulting from our corrections. In other words, the linear component of the spatial phase corrections has to be estimated. Figure 4.1 illustrates a typical phase correction pattern. Because of the modulo 2π nature of phase measurements, 2π phase jumps often occur as shown in Figure 4.1(a). To estimate the linear phase component, a direct approach would try to fit a straight line thorough the phase corrections using linear regression. Such straight line fitting would only be meaningful after removing all 2π jumps. This process, illustrated in Figure 4.1(b), is referred to as "phase unwrapping." Because recognizing a 2π phase jump involves setting a threshold and making a decision, the process could be unreliable depending on the following two factors:

22

(1) The range over which phase errors due to ionospheric distortion vary from element to element.

(2) The slope of the underlying straight line.

Since the direct methods of phase unwrapping are unreliable, a better technique for estimating the linear phase term was developed. First, the phase corrections are represented as phasors of unity magnitude. Then, the phasor sequence is Fourier transformed using an FFT, and an estimate of the linear phase term is obtained from the location of the peak in the Fourier domain. Of course, this technique is not completely error-free. The Fourier transform will exhibit a well-defined peak, or mainlobe, only when phase corrections vary over a finite interval around the underlying linear term. However, our technique is by far more robust, as opposed to a threshold-based direct phase-unwrapping method, because a single large phase excursion, or even several such excursions, cannot significantly change the end result

5. EXPERIMENTAL RESULTS

5.1 Estimation of Correlation Distance and Correlation Time

As mentioned before, ionospheric propagation randomly spreads both the target and clutter energy in time and space. The objective of this effort is determine whether application of self cohering techniques can use clutter echoes to compensate this wavefront distortion, resulting in:

(1) Increased echo strengths at the array output.
(2) Lower sidelobe levels in the azimuth domain.
(3) Lower sidelobe levels in the Doppler domain.
(4) Smaller spreading of clutter energy in Doppler space.

This section presents direct evidence that items (1), (3), and (4) are true; the truth of (2) can only be inferred, since a beacon is required for conclusive proof.

Echoes from clutter and targets at different ranges travel through different portions of the ionosphere, and, hence, undergo different distortions. To first order, the wavefront distortion caused by ionospheric propagation can be assumed to be the same over a given range interval. The length of this range interval, or *correlation distance*, over which distortion can be assumed constant, depends on how rapidly the characteristics of the ionosphere change in space. The phase corrections derived using self cohering techniques can be applied to data from ranges that are within a correlation distance of each other. Further, the clutter data from which these phase corrections are derived must also be from the ranges that are within a correlation distance of each other. In other words, the self cohering techniques should derive the phase corrections using data from ranges that are within a correlation distance of each other, and apply these phase corrections to the same data set.

Motion of the ionosphere causes the distortion of the echoes from a particular range to vary with time. To first order, we may assume that the distortion is constant over a certain time interval, called the *correlation time*. Only the data collected within this correlation time can be used to derive the *spatial* self cohering phase corrections across the array. Further, these corrections are applicable only to the data collected during this time interval.

As mentioned in Section 2, averaging over sweeps is performed first for the SCA to increase the clutter-to-noise ratio prior to spatial cohering. This corresponds to first doing Doppler processing at the element, or subarray, level and then applying the SCA to the zero Doppler data. For the TCA, averaging over elements is done before processing data from successive sweeps. This corresponds to first beamforming and then applying the TCA to the beamformed output because the data at the element level is too noisy and produces poor directivity. When both the TCA and the SCA are used together, the beamforming is best done after applying the SCA and prior to the TCA.

24

As previously pointed out, the number of range cells used to estimate the correlation must be large enough to provide a good estimate, but small enough so that the quantity being estimated remains relatively constant over the range interval used. The number of sweeps averaged over before using the SCA must be large enough to increase the clutter-to-noise ratio, but it must be smaller than the coherence time of the medium. This temporal coherence may be improved slightly by the TCA at the element level. The number of elements averaged before final application of the TCA must be large, but it must not exceed the spatial coherence of the received data. Be applying the SCA first, we found that all 36 elements could be used in this step. Given the large number of processing alternatives, we varied the parameters to maximize the peak processed clutter return at zero Doppler. Using this criterion, we found that the correlation distance varied from 4 to 5 range bins and the correlation time varied from 16 to 32 sweeps depending on the particular set being processed. The manner in which the data were processed is described next in detail.

5.2 Data Processing Method

Figure 5.1 depicts the basic data processing method. The groundwave signal from the transmitter at Ava is used to determine the absolute range, and the range bins corresponding to clutter echoes are identified based on echo strength and Doppler content. The received data, consisting of complex data samples from a large number of range bins and 64 sweeps at each element, is partitioned into segments of ΔN_r range bins and ΔN_s sweeps. Figure 5.1 assumes that $\Delta N_r = 5$ range bins and $\Delta N_s = 16$ sweeps.

According to Figure 5.1, the Spatial Correlation Algorithm, or one its variations (iterative or multiple lag), is applied to each segment of data as follows. First the SNR in the data for ΔN_s sweeps from each range bin, at each element, is increased using a ΔN_s-point FFT. The FFT output for the zero Doppler cell, for each of the ΔN_r range bins, is used to determine the phase corrections at each element. The linear phase term is removed from the spatial phase corrections to maintain consistency of the look direction over the entire coherent dwell. Phase unwrapping is required for this step. The resulting phase corrections are used for forming multiple beams with the data for all ΔN_s sweeps and all ΔN_r range cells. This process is repeated until all sweeps and range bins are processed.

The Temporal Correlation Algorithm is applied to the beam outputs because the SNR is not sufficient to apply the TCA at the element level. Also, after beamforming, the illuminated sector is resolved into smaller azimuth cells resulting in a better match to the azimuthal dependence of the ionospheric phase instabilities. For a given output beam, the TCA is used to determine the temporal phase corrections for all 64 sweeps using the data from ΔN_r adjacent range bins. These phase corrections are then Fourier transformed using an FFT to produce a range-Doppler map for each range, for a given output beam. The results of applying the various algorithms to correct for ionospheric propagation effects are described below.

Figure 5.1. Data Processing Method.

The flowchart contains the following boxes and labels:

range FFT
- circulary shift Ava ground wave to starting range
- pick the the range bin interval corresponding to ground clutter

partition data into chunks of 5 range bins and 16 sweeps

doppler FFT over 16 sweeps to build the SNR

Apply the SCA over the 5 range bin interval and zero doppler cell
- unwrap phase corrections
- apply the same phase corrections across the 36-element array for all of the 5 range bins and 16 sweeps of the current data chunk

FFT beamform at all ground clutter range bins and all sweeps

Pick a particular beam position

Apply the TCA over 5 range bin intervals but for all sweeps

Doppler FFT to produce a range doppler map

move to the next 16 sweep chunk until all 64 sweeps are processed

move to the next 5 range bin chunk until the full ground clutter interval is processed
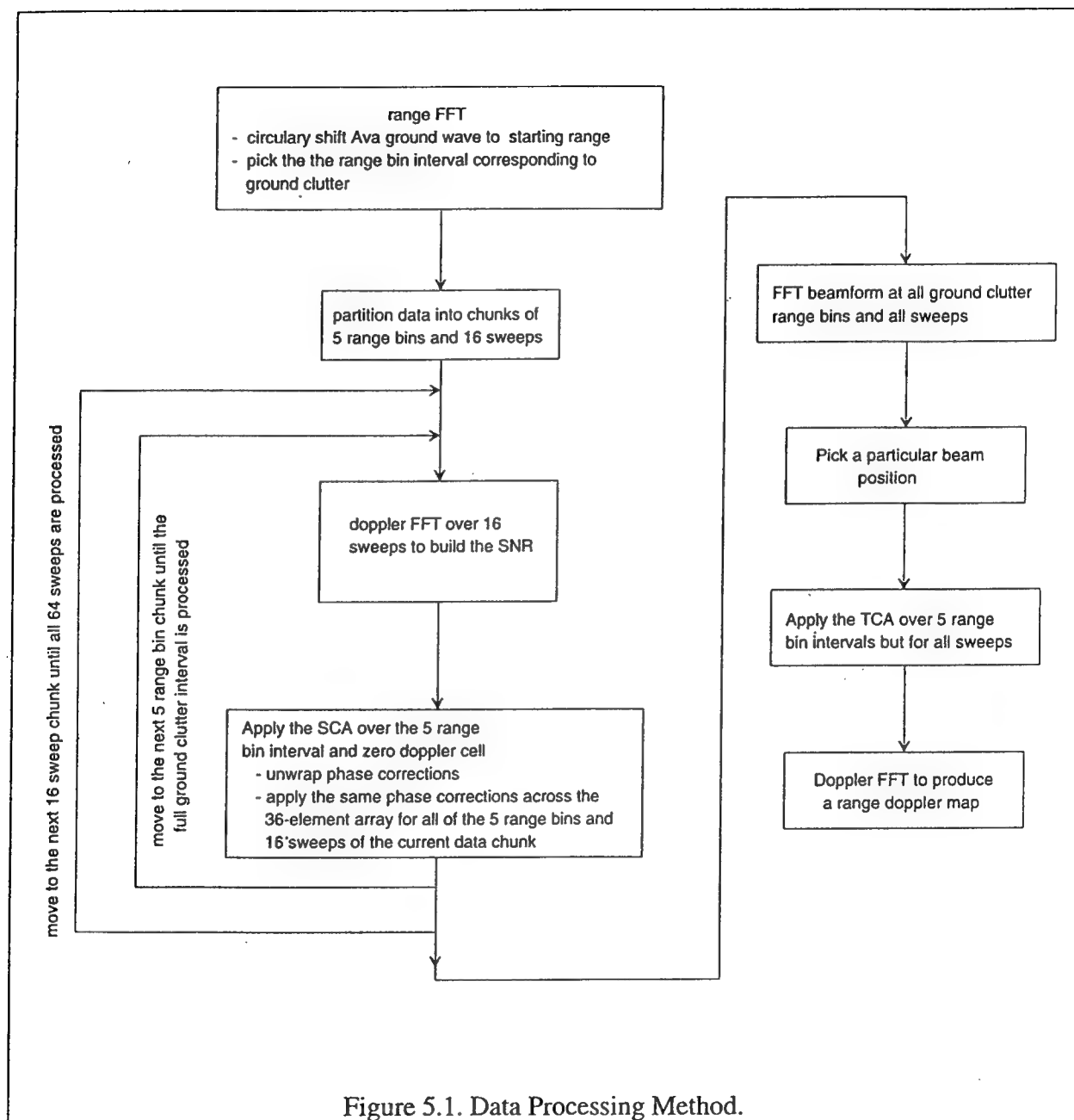
## 5.3 Processing for the Nov01504 Data Set

5.3.1 Data Description

The data set labeled Nov01504 was collected using a 2.5-second, 64-pulse coherent dwell. It consisted of 81 sweeps of complex data at 36 elements with 400 frequency samples per sweep. Also furnished was a calibration file of 36 complex values based on the range and Doppler resolved groundwave due to the transmitter at Ava, NY. As described in Section 3.1, the data contained a severe transient starting at frequency sample 219. After introducing the nonlinear correction discussed in Section 3.2, we are able to use 378 samples instead of the usual 200 in the range FFT, improving range resolution by 90% (16 km instead of 30 km). Also, sweep-to-sweep array calibration based on the Ava groundwave was performed to eliminate time varying system errors and focus our attention on ionospheric distortion as described in Section 3.3. The data contained surface clutter returns from HF backscattered signals collected at Verona, NY in the presence of serious ionospheric distortion. The data were processed at GORCA on a 486 IBM PC and a SUN Sparc II workstation.

5.3.2 Results

Figure 5.2 shows a number of range-Doppler maps that summarize many of the important results from the Nov01504 data set. All the maps in Figure 5.2 are produced based on a look angle midway between beam 10 and beam 11 of the receive array [5]. This look angle corresponds roughly to the centroid of illuminated ground clutter and hence spatial corrections, obtained without subarray processing, are best matched to this direction. Strip 1 is a range-Doppler map of the original data after enhancing its range resolution by correcting the transient at frequency sample 219. Strip 2 is produced after correcting for the relative phase jitter between the Ava transmitter and the receiver LO. Sweep-to-sweep phase and amplitude corrections are derived from the range-resolved transmitter groundwave and applied across the receive array as described in Section 3.3. Only a minor improvement in Doppler spread and Doppler sidelobes is observable. This suggests that the phase errors due to ionospheric distortion dominate this data set. For a precise evaluation of the improvements offered by the self cohering algorithms, we performed this sweep-to-sweep pre-calibration to remove system errors in all the results presented in this report.

Strip 3 resulted from applying the ISCA [18] spatially and the Iterative TCA (ITCA) temporally, based on segments of $\Delta N_r = 5$ range bins and $\Delta N_s = 32$ sweeps. A signifcant reduction in the Doppler spread of the ground clutter is obvious. The midsection of the transmitter footprint showed a modest improvement. Greater improvements were obtained toward the two ends of the beam footprint. A dramatic reduction in Doppler spread is evident at and beyond the far end of the beam footprint. This part of the illuminated ground is shown in Figure 5.2 as strips 1' through 4', where we matched the gray scale to its dynamic range for clarity. It should be noted that while we originally

thought that this range interval corresponds to the far end of the transmitter footprint, discussions with Rome Laboratory/ERCP suggested that energy in this range interval is due to ground backscatter coming from rays refracted through the ionospheric "blob" at 1160-1688 km. We believe that this region of the backscattered signal is a good example of the phenomenon of spread-Doppler clutter. In strip 4 we took $\Delta N_r = 6$ and left $\Delta N_s = 32$ as before. A slight deterioration in Doppler spread, relative to strip 3, may be noticed.

Figure 5.2. Range-Doppler Maps From the Nov01504 Data Set.
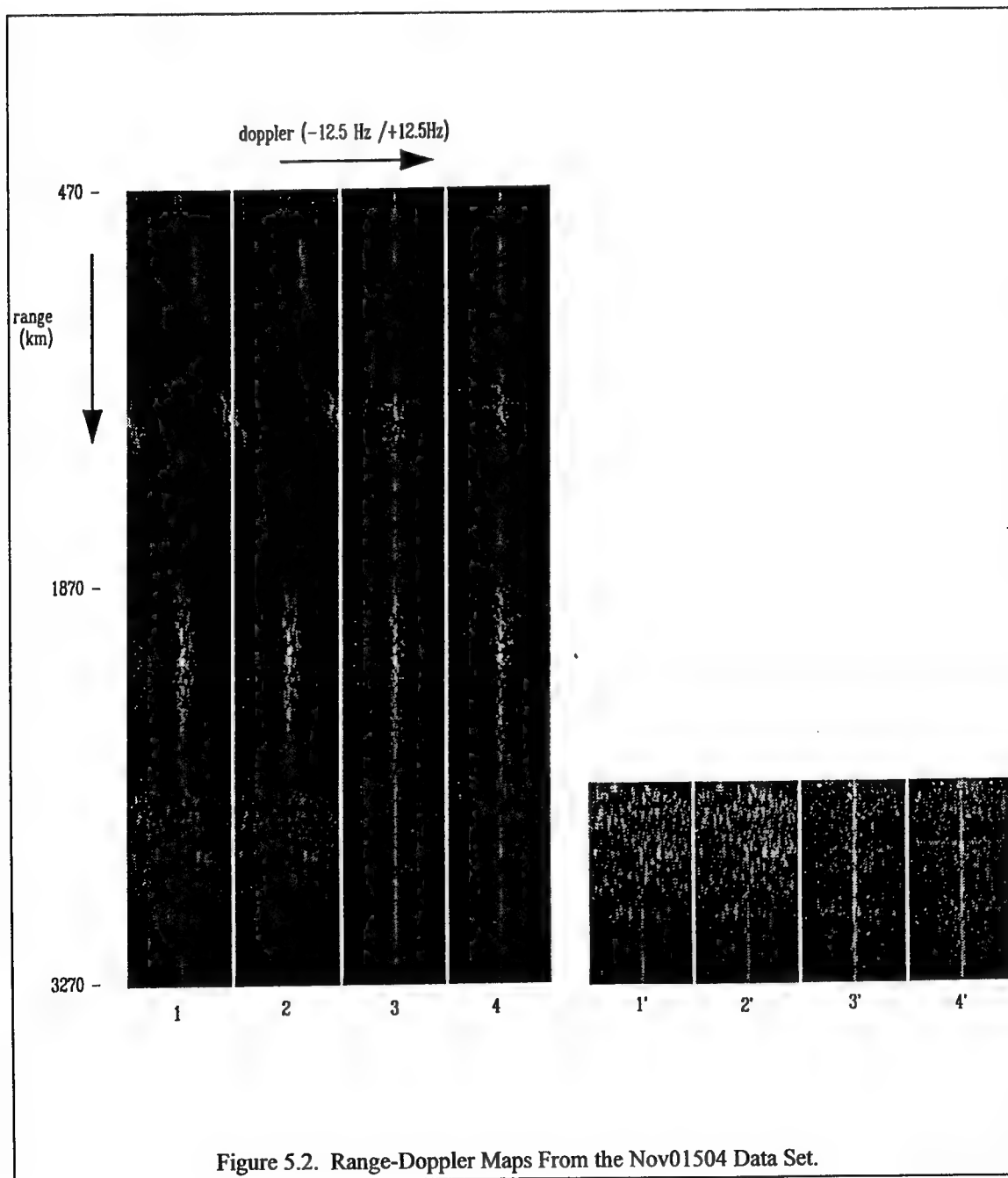
Observe that, similar to losing the absolute azimuth position after direct application of the spatial phase correction, the mean Doppler shift has been automatically removed at all ranges. This has no effect on ground backscatter because its mean Doppler shift is zero to start with. Unfortunately, ionospheric returns also lose their mean Doppler shifts, which contain information of interest to Rome Laboratory scientists. In Section 5.6, we use our new method of phase unwrapping, described in Section 4, to estimate the linear phase term in our temporal (sweep-to-sweep) phase corrections so that we can register ionospheric returns at their absolute Doppler.

Figures 5.3 through 5.13 show Doppler spectra cuts averaged over 5 range bins to provide a more quantitative evaluation of the results of Figure 5.2. Solid curves show the "before" case (strip 2) and dotted curves show the "after" case (strip 3). The Doppler cut of Figure 5.3 is obtained from the near end of the transmitter footprint. An improvement in Doppler spread is evident. Figure 5.4 is produced from the mid-section of the transmit beam footprint. Doppler spread was reduced by almost a factor of two while a reduction in Doppler sidelobes corresponding to an improvement in subclutter visibility of about 2 dB is evident. The apparently small loss at zero Doppler in Figure 5.5, at about three-quarters into the footprint, is due to the coarse sampling used in computing the Doppler spectrum. Better results were obtained toward the far end of the footprint as can be seen in Figures 5.6 and 5.7. Figure 5.6 shows a reduction in Doppler spread of better than 100% combined with overall gain improvement of about 9 dB at zero Doppler.
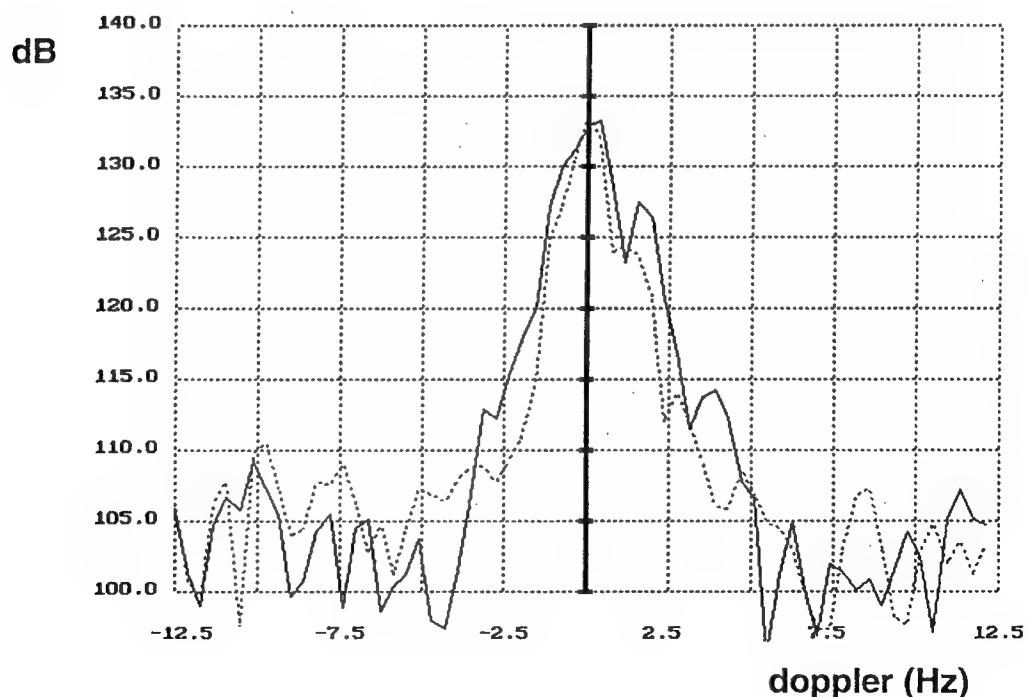

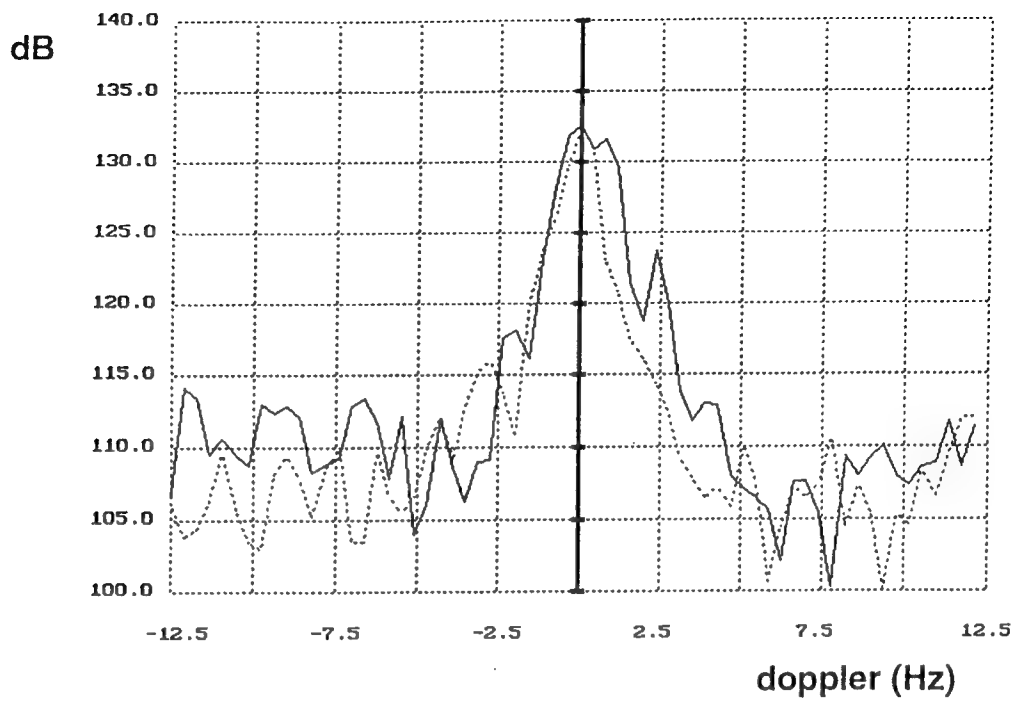Figure 5.3. Averaged Doppler Cuts (1934-1980 km).

Figure 5.4.   Averaged Doppler Cuts (2168-2215 km).
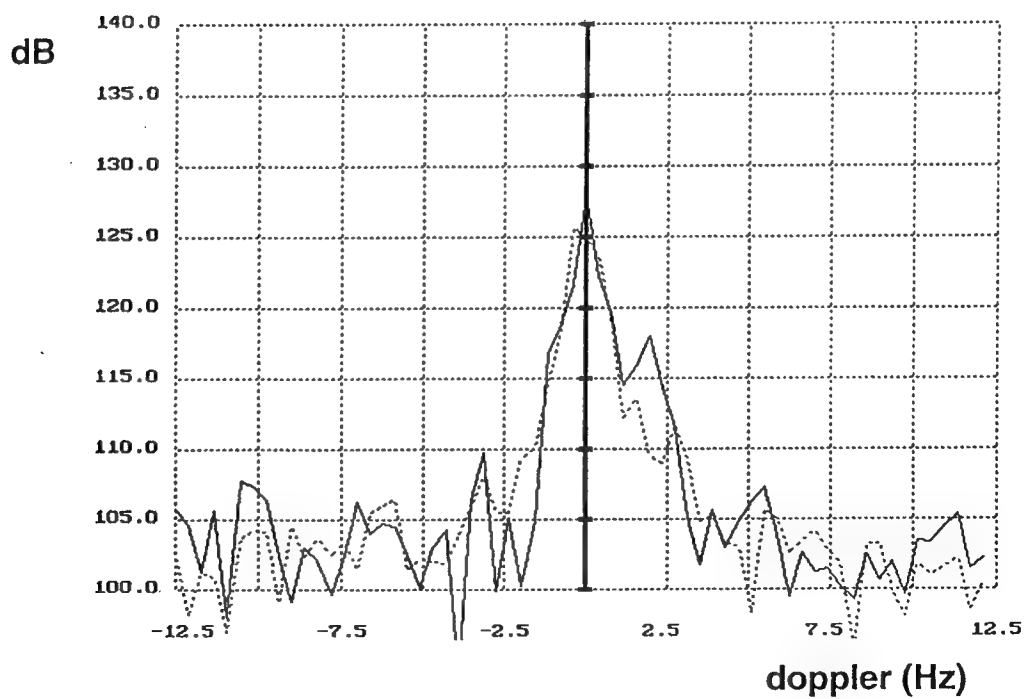

Figure 5.5.   Averaged Doppler Cuts (2344-2391 km).

Figure 5.6.   Averaged Doppler Cuts (2402-2449 km).

Figure 5.7.   Averaged Doppler Cuts (2461-2520 km).

Figure 5.8. Averaged Doppler Cuts (2578-2637 km).
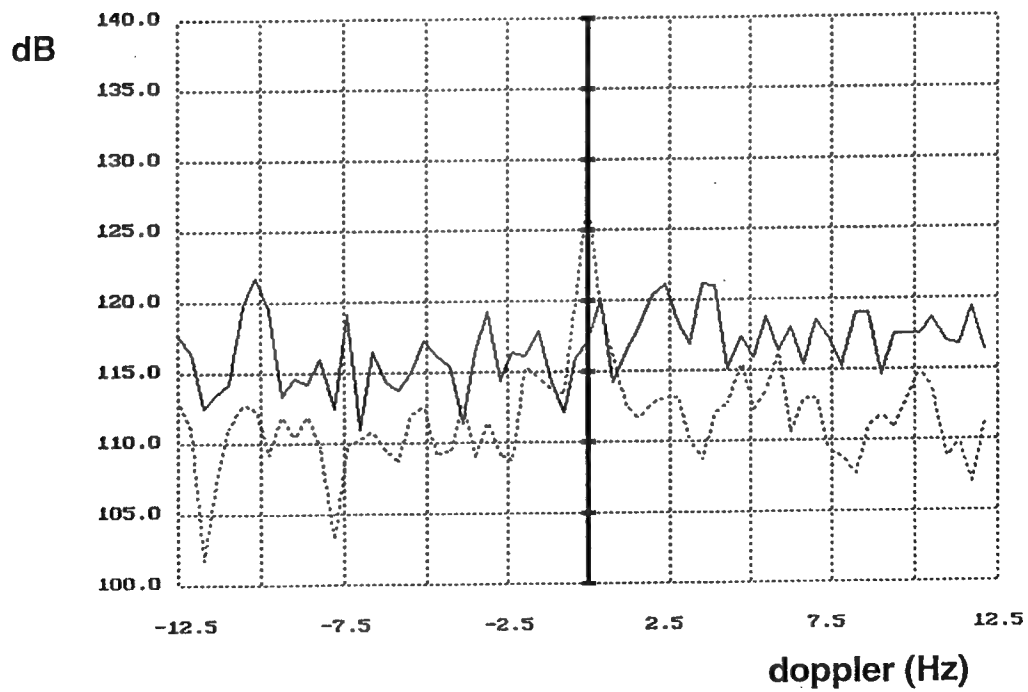
Figure 5.9. Averaged Doppler Cuts (2637-2684 km).

32
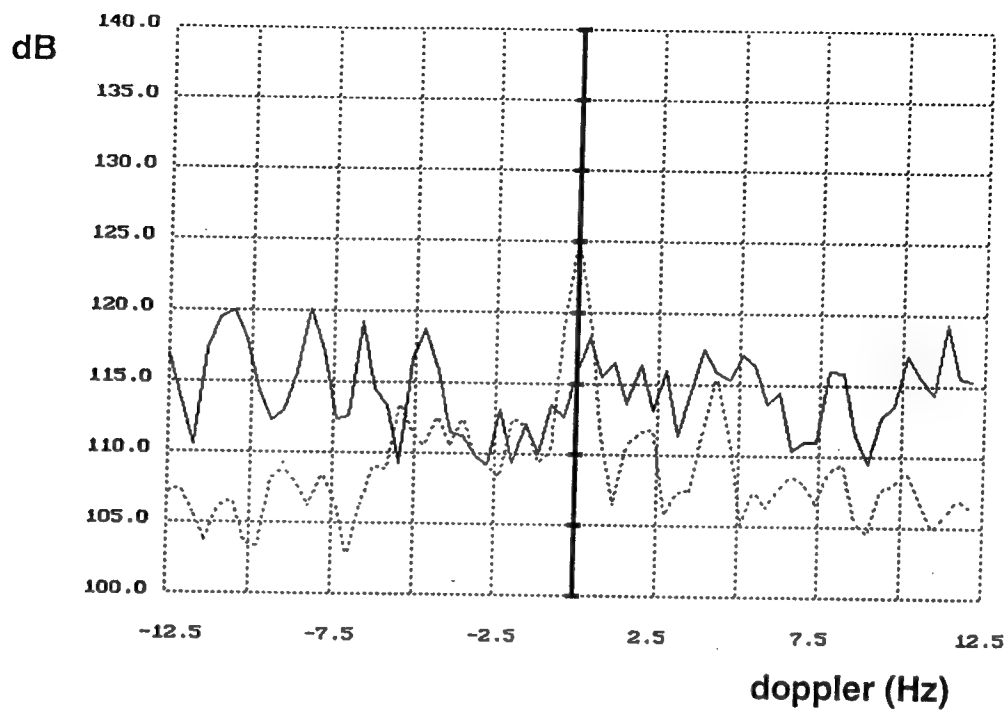
Figure 5.10. Averaged Doppler Cuts (2695-2742 km).
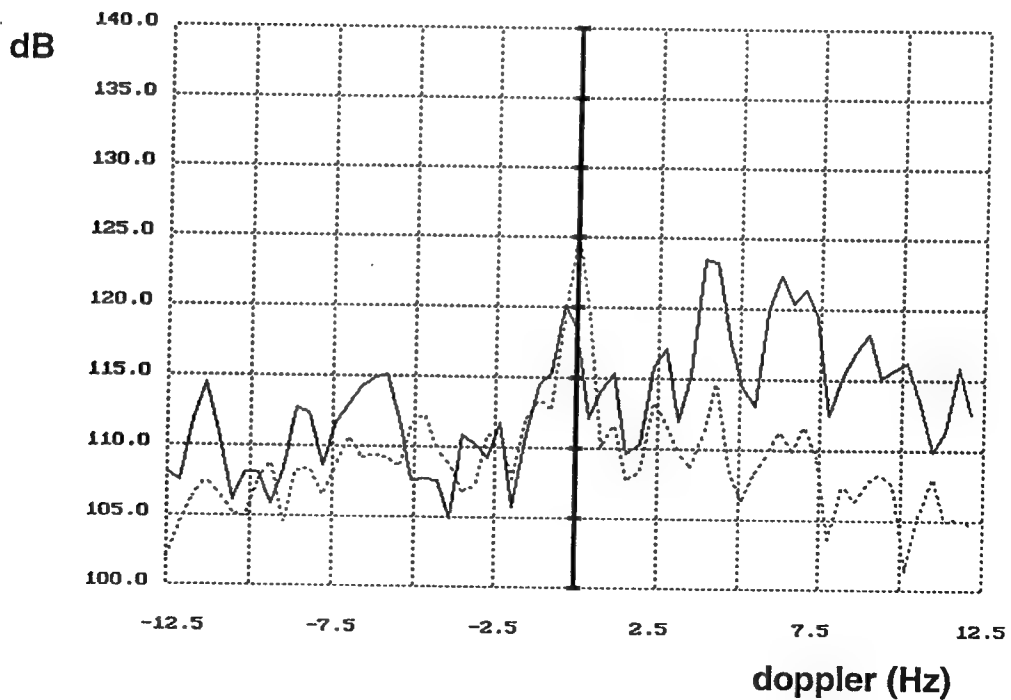
Figure 5.11. Averaged Doppler Cuts (2813-2859 km).
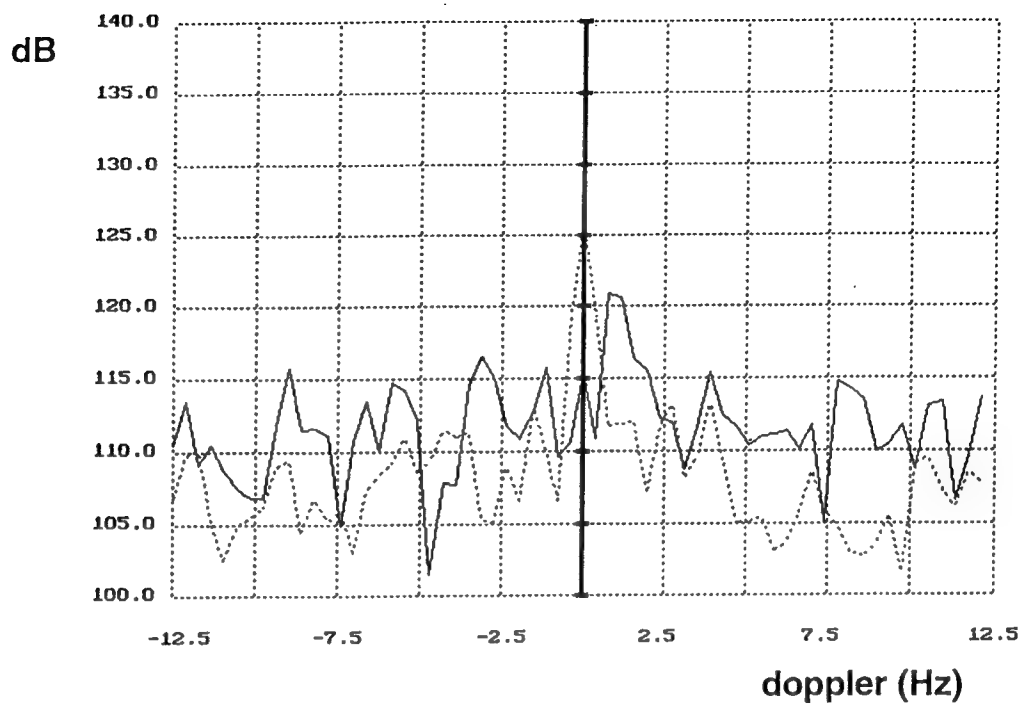
Figure 5.12. Averaged Doppler Cuts (2871-2918 km).

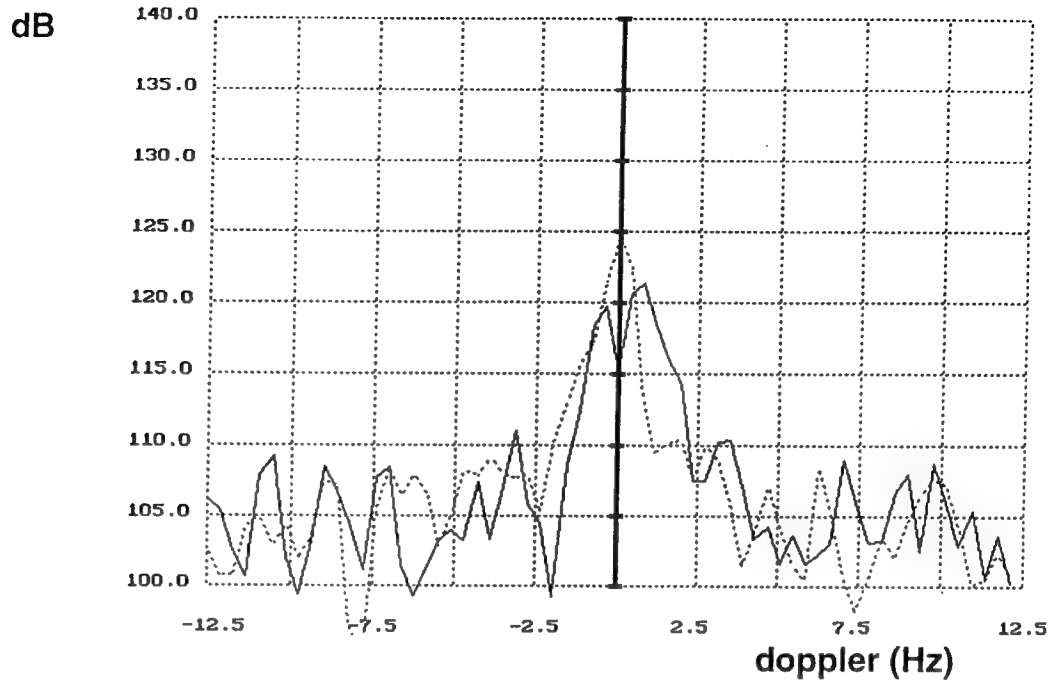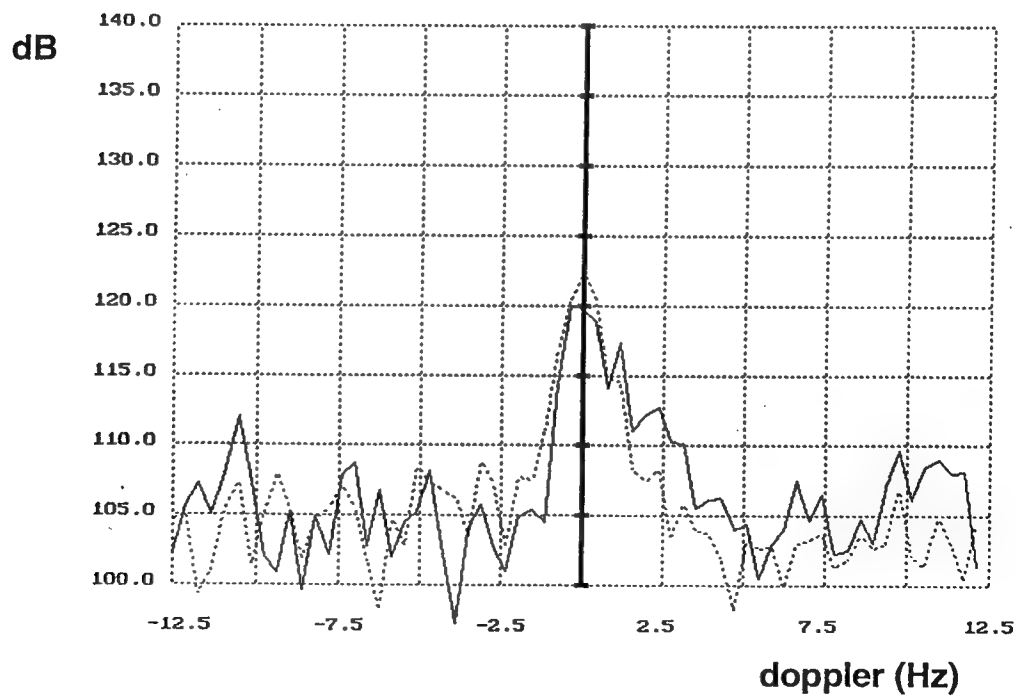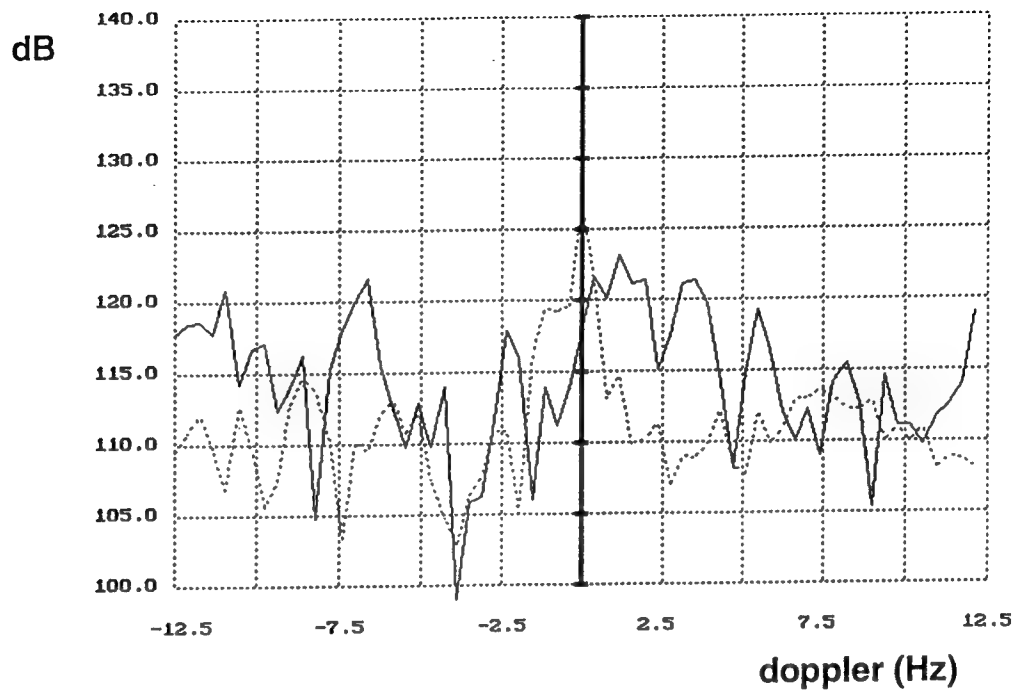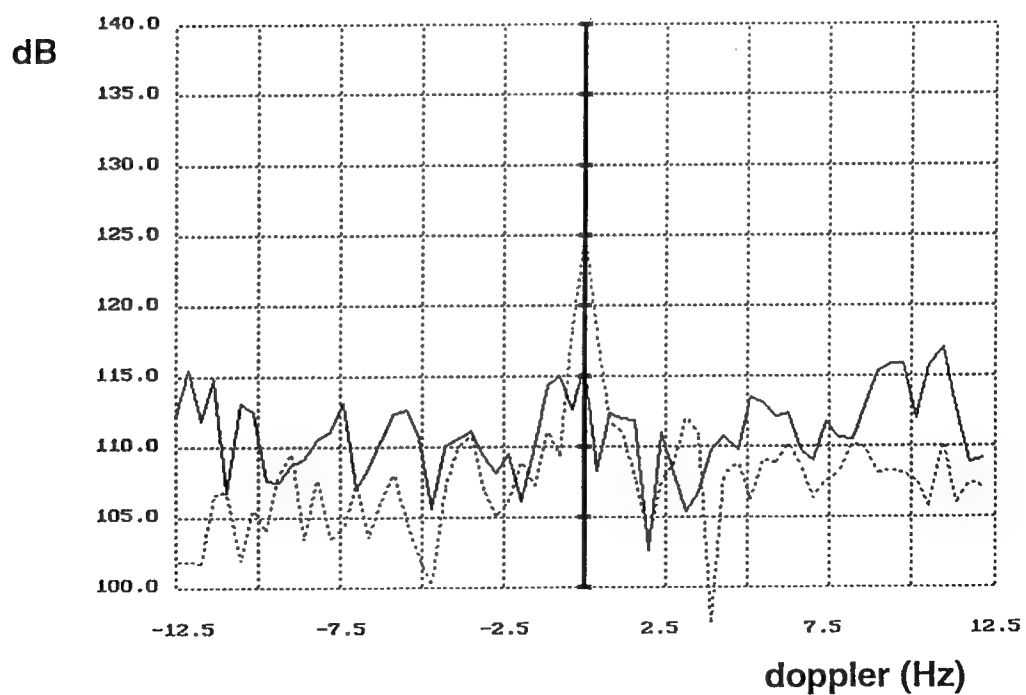Figure 5.13. Averaged Doppler Cuts (2930-2977 km).

34

Our most dramatic results were obtained in the spread-Doppler clutter region as manifested in Figures 5.8 through 5.13 where the improvement appears to be limited only by the noise floor at about 107 dB. Except for Figure 5.8, the resulting Doppler spread is limited by the length of the coherent dwell as ideally should be the case. It is believed that the improvement in Doppler spread was not dramatic in Figure 5.8 because it represents a transitional region where two propagation paths coexisted: (1) remnants of the far end of the usual transmitter footprint; plus (2) energy refracted from the ionospheric turbulence responsible for the spread-Doppler clutter.
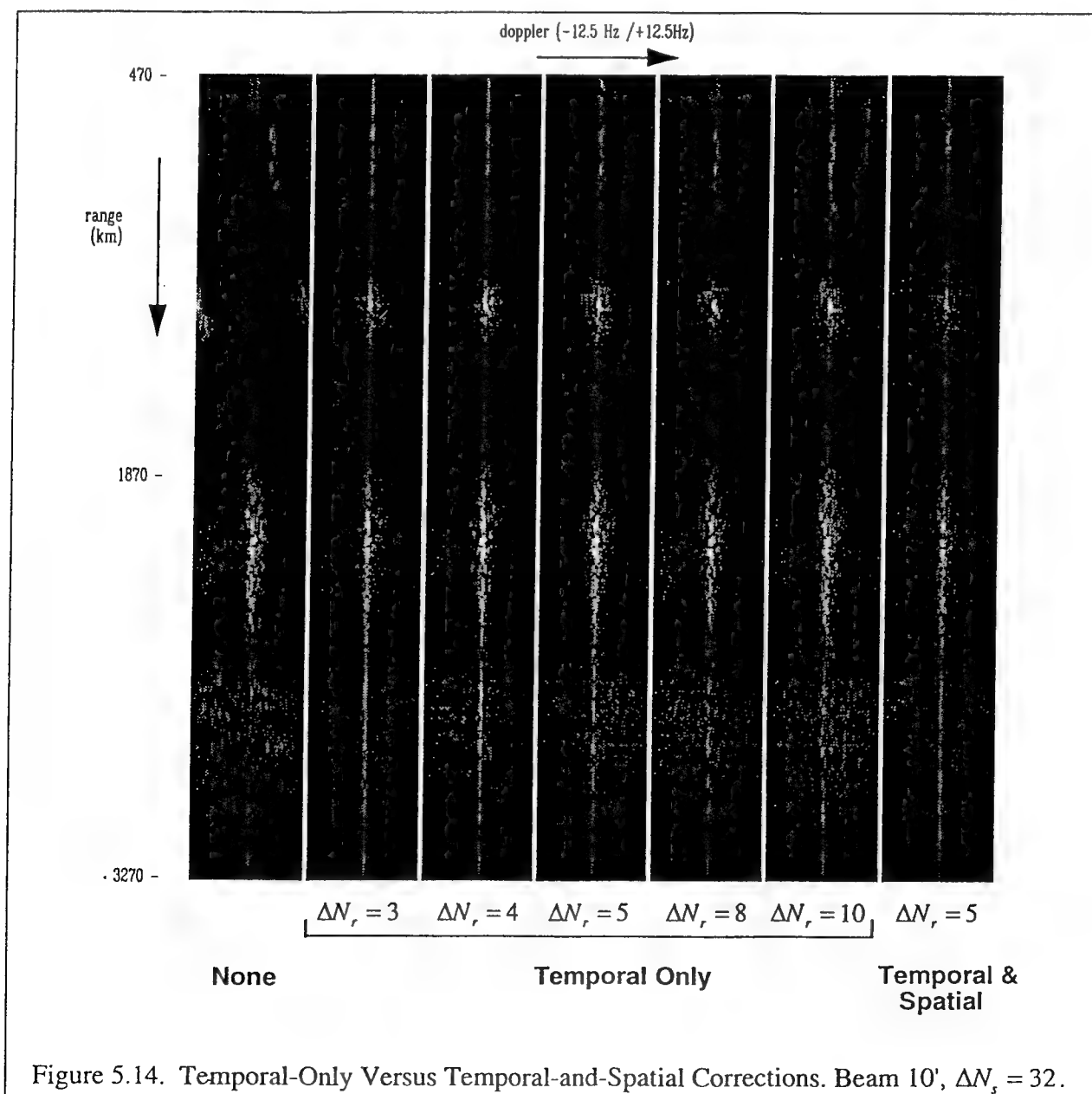
Figure 5.14. Temporal-Only Versus Temporal-and-Spatial Corrections. Beam 10', $\Delta N_s = 32$.

To check the validity of these improvements, Figure 5.14 was produced where all but the left-most and right-most strips were made by applying temporal corrections only. This way there is no doubt that the "before" and "after" maps correspond to the same look direction. We completely avoid any problems that may arise due to the limited reliability of methods of phase unwrapping needed to remove the linear phase term of spatial phase corrections. Notice that "temporal-only" corrections are consistent with previous results. The trend of reducing the Doppler spread towards the far end of the transmit beam and in the spread-Doppler region is quite clear. It is important to compare the two $\Delta N_r = 5$ strips at the middle and the right end of Figure 5.14. The only difference between these two strips is the application of spatial corrections to the right-most strip. The obvious added improvement in Doppler spread due to spatial corrections gives a strong indication of the stabilization of the spatial array pattern from sweep-to-sweep. Also, comparing the zero-Doppler response of these two strips, an average increase of about 1 dB due to spatial corrections alone was found. Consistency of the array pattern from sweep-to-sweep and increased gain due to spatial processing are strong indications of a significant improvement of the spatial pattern of the receive array. Therefore, in addition to improving the temporal coherence of the system, which is directly demonstrated in Figures 5.2 through 5.13, a significant improvement in spatial coherence can be inferred.

As explained in Section 5.1, increasing the size of ΔN_r beyond the correlation distance in range can be counter-productive with regard to our effort to decrease the Doppler spread. This effect can be seen in Figure 5.14. Also, decreasing the value ΔN_r increases the variance of the estimated phase corrections. It is important to note that decreasing ΔN_r to a very small value can lead to misleading results. Assuming no amplitude variation from sweep to sweep, it is straightforward to show that if we go to the extreme of taking $\Delta N_r = 1$, Doppler spread always vanishes irrespective of how much phase distortion we originally had. In this case, at each range bin of the receive beam under consideration, temporal phase corrections will be the conjugate of the phase of the original data. To guard against this effect, the choice of ΔN_r was never lowered below $\Delta N_r = 4$ in the remainder of this effort. This conclusion was supported by applying the processing chain of Figure 5.1 to pure random noise to check the validity of the Doppler narrowing properties of the self-cohering algorithms as detailed in Section 5.7.

Figure 5.15 shows the original range-Doppler-azimuth map. Notice the strong correlation between the position in range of the ionospheric blob at about one-third of the displayed range interval and the spread-Doppler clutter at about twice its range as observed over beam positions 6′ through 13′. There is also strong correlation between the strength of this moving ionospheric disturbance and the resulting spread-Doppler clutter. A moving picture of this region, generated by David Choi of Rome Laboratory from a number of successive data sets taken 3 minutes apart demonstrated this correlation in a more dramatic way. This strengthened the belief that the spread-Doppler clutter we processed is due to energy refracted through this particular ionospheric turbulence. Notice that the azimuth extent of the ionospheric turbulence is significantly smaller than that of the ground clutter illuminated by the transmitter footprint through the dominant first-hop

Figure 5.15. Original Range-Doppler-Azimuth Map. Beam Position b' = b + 2.6 Degrees.
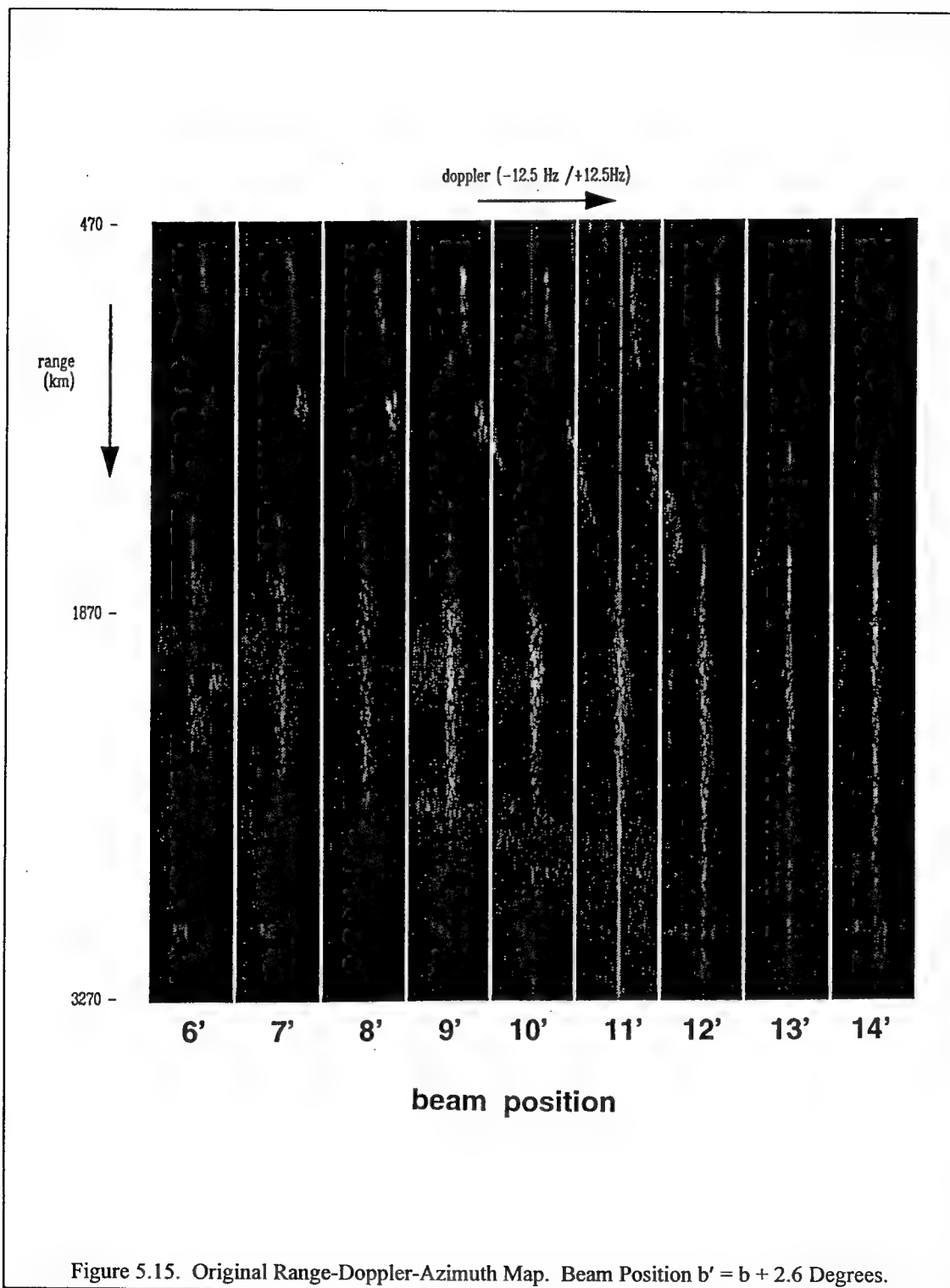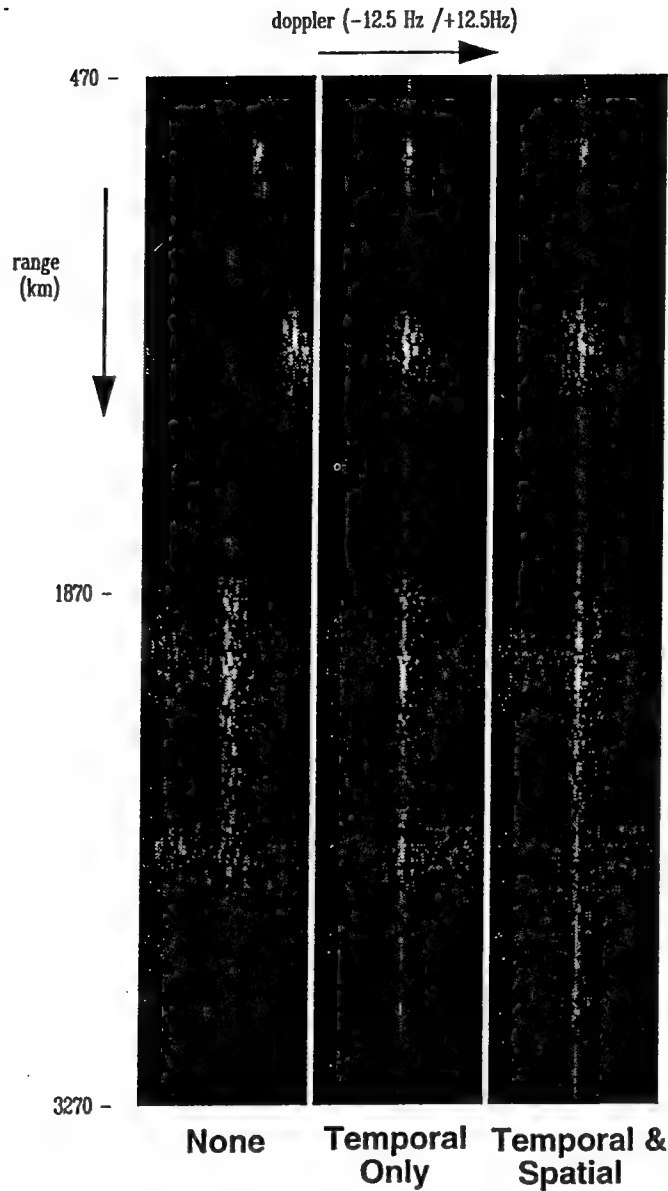
Figure 5.16. Range-Doppler Maps Produced from Beam Position 9'. $\Delta N_r = 5$, $\Delta N_s = 32$.

path. Moreover, because of the apparent oblique orientation of the turbulence, the resulting spread-Doppler clutter at any particular range has an even smaller azimuth extent. As explained in Section 4, reducing the azimuth extent of the illuminated clutter increases the intrinsic spatial correlation distance of the clutter returns at the receive aperture, and, hence, improves the accuracy of the resulting phase corrections. This explains why our most dramatic results are obtained in this region.

Figure 5.16 shows three range-Doppler maps produced from beam 9'. Because our spatial corrections pertain to a beamforming angle close to beam 10' (where the transmit beam is pointing), steering to beam 9' results in less improvement in Doppler spread. However, gain improvement at zero Doppler at long ranges is still apparent. It is believed that a 14-degree transmit beam is too wide. To improve the quality of phase corrections at an arbitrary look angle, the subarray processing technique in Section 4.2 was developed where the receive array is divided into overlapping subarrays to provide directivity to the process of deriving spatial phase corrections. Figure 5.17 shows the results of applying subarray processing to the Nov01504 data. The figure consists of range-Doppler-azimuth maps for beams 7' through 14'. The horizontal axis of each strip spans the Doppler interval -12.5 to 12.5 Hz. Range starts at 470 km (at the top of each strip). Range bin segment size is $\Delta N_r = 5$, and sweep segment size is $\Delta N_s = 32$. The upper sequence of maps of Figure 5.17(a) shows the original data without corrections. Except for a small shift in gray scale and the inclusion of beam 6', Figures 5.15 and 5.17(a) are identical. The lower sequence of maps of Figure 5.17(b) shows the same data after spatial and temporal corrections are applied. An average increase in gain of about 1.5 to 2.5 dB was observed in the main ground backscatter region at every beam position. Most beam positions exhibit a noticeable reduction in Doppler spread. The reduction in Doppler bandwidth is most obvious in beams 7' and 8'. Significant improvements in the spread-Doppler clutter can be seen in beams 7' through 10'. Refer to Figure 5.15 for a look at this region with finer amplitude resolution. The small range interval within the spread-Doppler clutter region of beam 9' is believed to be due to the coexistence of two propagation paths as explained with regard to Figure 5.8.

A very significant improvement is evident in the spread-Doppler clutter region of beam 10'. However, the improvement is somewhat less dramatic than that obtained in Figure 5.2. The reason is that while the subarray processing technique employed in Figure 5.17(b) makes it possible to change the look direction at will, the accuracy of the resulting phase corrections is inferior to that produced by the ISCA [18]. The ISCA, used to produce Figure 5.2, takes into account element-to-element phase errors which are completely ignored by the subarray processing method. As a result, phase corrections produced by the ISCA are well matched to the direction of the centroid of illuminated ground clutter, which happens to be very close to beam position 10', and that is why the ISCA performed better at this particular angle. Beam 11' has a unique problem; it is the beam closest to the direction of the transmitter at Ava. The narrow vertical line at zero Doppler in beam 11' of Figure 5.17(b) is due to leakage of the transmitter groundwave through range sidelobes. This signal has nothing to do with ionospheric effects and can only corrupt phase corrections obtained from ground backscatter as evident in beam 11' of Figure 5.17(b).

39
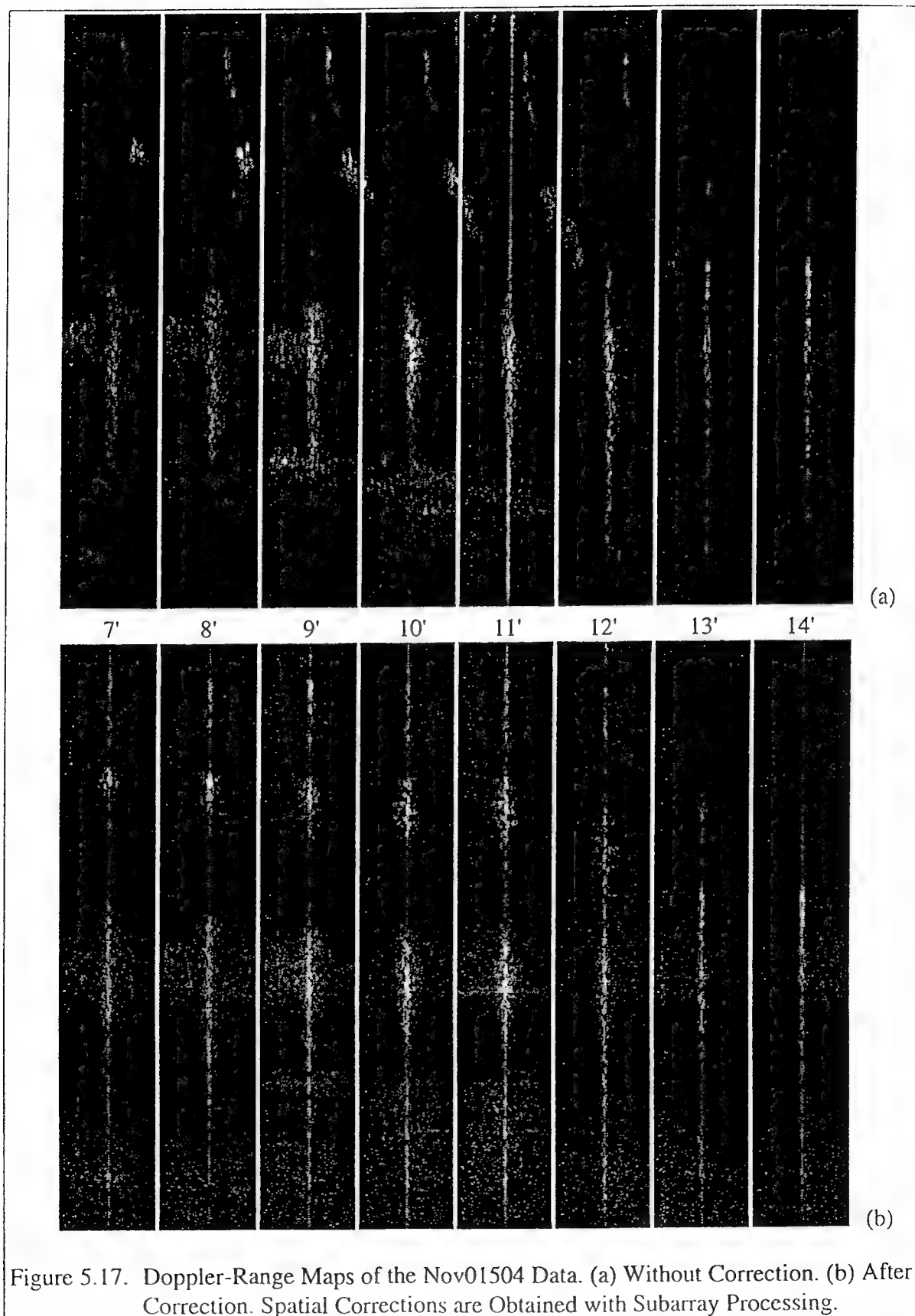
Figure 5.17. Doppler-Range Maps of the Nov01504 Data. (a) Without Correction. (b) After Correction. Spatial Corrections are Obtained with Subarray Processing.

5.3.3 Propagation Factors Affecting Self-Cohering Performance

Figure 5.18 illustrates a greatly simplified model of refraction by the ionosphere. The model is intended only for the purpose of illustrating the importance of fine range resolution and explaining some of the preceding results. Because the transmitter footprint is narrower towards its near and far edges, two beneficial factors come to play at the two edges:

(1) The intrinsic spatial correlation distance of ground backscatter increases across the receive aperture making our phase estimates more precise.
(2) The azimuth extent of the illuminated ionosphere decreases, making our corrections more meaningful as they pertain more to the transient beam pointing angle.

Figure 5.18. A Greatly Simplified Model for Refraction by the Ionosphere. Transmitter Beam Has an Angular Extent $\theta_2 - \theta_1$.

Also, from the geometry, it is straightforward to show that the number of range bins passing through the same ionospheric irregularity at the far end of the transmitter footprint is

$$\Delta N_{r_1} \approx \frac{\Delta\theta_1}{\delta\theta_1} = \frac{2l_z \cos\theta_1}{\Delta R \tan\theta_1}$$

where

$\Delta\theta_1$ = angle subtended by an ionospheric irregularity of vertical size l_z, and
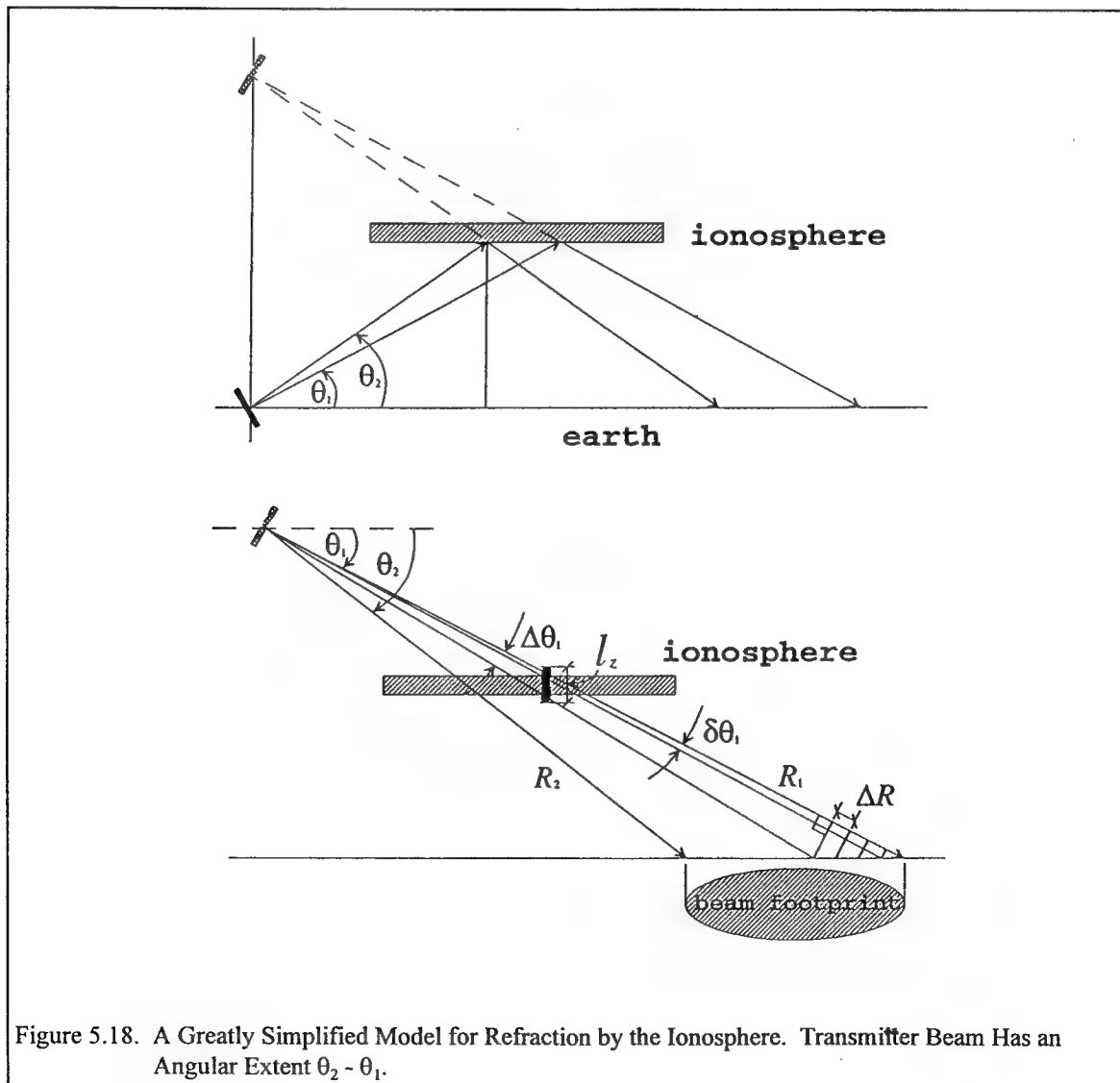
$\delta\theta_1$ = angle subtended by a range resolution cell of size ΔR.

For example, with l_z = 6 km and ΔR = 15 km, towards the far end of the transmit beam, θ_1 = 8 degrees, yielding ΔN_{r_1} = 5.6. Similarly, towards the near end of the transmit beam θ_2 = 22 degrees, and we obtain ΔN_{r_2} = 1.8. Thus, more range bins are available at the far end. This explains why we obtained better results towards the far end of the transmit beam.

5.4. Processing Results for the Sep24322 Data Set

5.4.1. Data Description

The data set labeled Sep24322 consisted of 64 sweeps of complex data at 36 array elements with only 200 frequency samples per sweep, thus limiting range resolution to 30 km. The transmitter frequency is 10.58 MHz. The data contained surface clutter returns from HF backscattered signals collected at Verona in the presence of modest ionospheric distortion. The data set is similar in every other respect to that described in Section 4.1.

5.4.2. Results

Figure 5.19 shows the results of applying both spatial and temporal corrections, ISCA + ITCA, to the Sep24322 data. The figure consists of Doppler-range maps for beams 5′ through 13′, where the corrected beam position b′ = b + 1.1 degrees and b is the original beam position as explained in Section 4.2. The horizontal axis of each strip spans the Doppler interval -12.5 to 12.5 Hz. On the vertical axis, range starts at 470 km at the top and ends at 5602 km at the bottom. The range bin segment is ΔN_r = 4 and the sweep segment is ΔN_s = 32. A smaller range bin segment was chosen because the 30 km range resolution of this data set is coarser than the 16 km range resolution used before.

The upper sequence of maps in Figure 5.19(a) shows the original data without corrections. The lower sequence of maps Figure 5.19(b) shows the same data after spatial and temporal corrections are applied. An average increase in gain of about 1-2 dB was observed in all beam positions. Most beam positions exhibit a noticeable reduction in

42

Doppler spread. The reductions in Doppler bandwidth are most dramatic in the double bounce area at the bottom third of each strip. The bright spot at about the middle of each strip of Figure 5.19(a) is due to the dc offset and appears shifted in Doppler due to the frequency difference between the transmitter and the LO at the receive array. We estimated the dc component and removed it in the data of Figure 5.19(b).

Proper self-cohering should have the following effects:

(1) Increased echo strengths at the array output.
(2) Lower Doppler sidelobe levels.
(3) Smaller spread of clutter energy in Doppler.

All three effects are evident in the range-Doppler maps of Figure 5.19. The large amount of spreading of the clutter energy into all Doppler bins is apparent when no self cohering is performed. Further, it is also obvious that these sidelobe artifacts are lowered as self cohering algorithms are used to correct for wavefront distortions. Besides lowering the sidelobe artifacts, self cohering also reduces the width of the Doppler mainlobe; i. e., it reduces the Doppler spread due to temporal variation of the distortion due to ionospheric propagation.

Figures 5.20 plots one-dimensional cuts of the range-Doppler maps of Figure 5.19. Each cut represents the result of averaging 5 consecutive range bins. The six graphs in the figure compare the Doppler responses before and after the application of self cohering. The lowering of the sidelobes and reduction of spread-Doppler clutter after the application of self cohering are evident from these figures. For example, the third graph of Figure 5.20 shows about 3 dB increase in processing gain at zero Doppler. The fourth graph shows a 2.5 dB processing gain accompanied by a significant decrease in Doppler spread. In the fifth and sixth graphs, Doppler resolution was restored to its theoretical limit where a reduction in Doppler spread of better than 50% was achieved. It should be noted that, compared with the results of the Nov01504 data set, results obtained from the Sep24322 data set were less dramatic because the September data had much less distortion to begin with.

5'	6'	7'	8'	9'	10'	11'	12'	13'

Figure 5.19. Range-Doppler OTH Radar Clutter Maps of the September Data. (a) Without Correction, (b) With Correction. Spatial Corrections are Obtained with Subarray Processing. The Gray Scale Displays 40 dB of Dynamic Range.

44
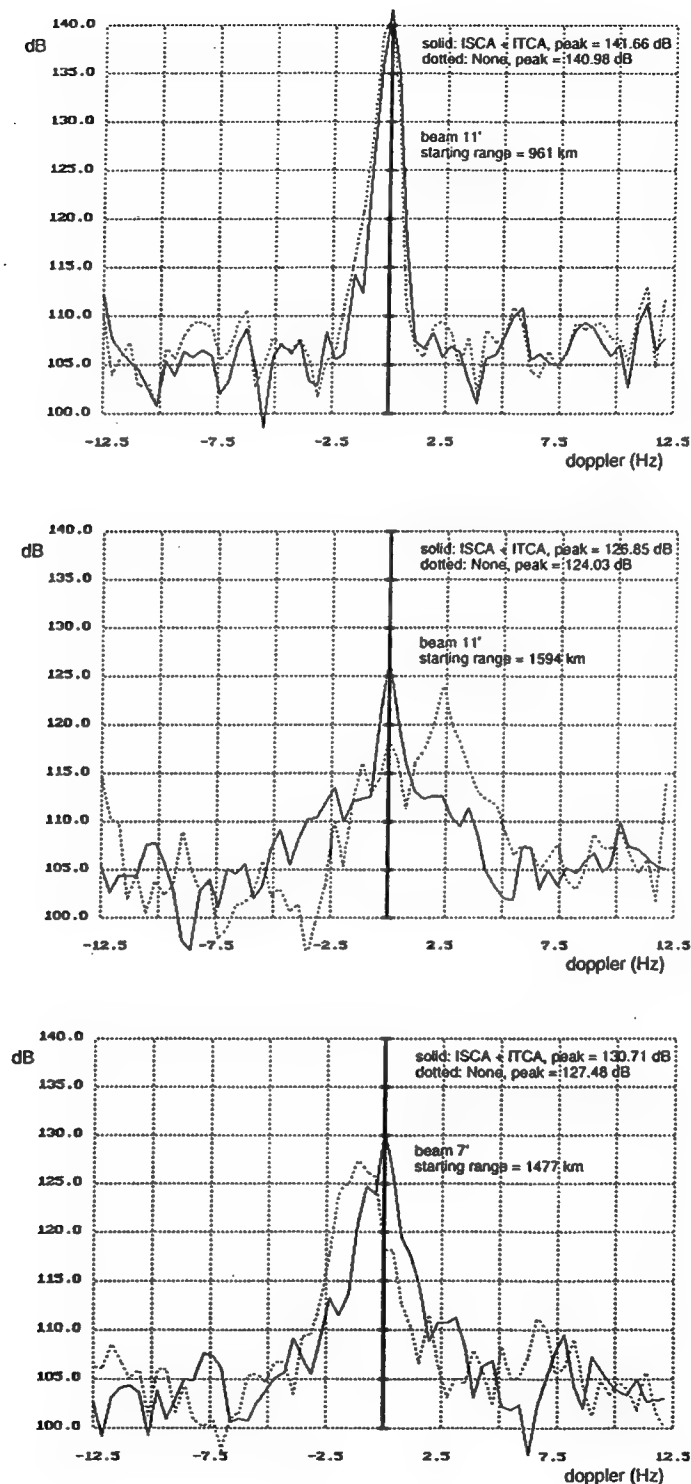
Figure 5.20. OTH Doppler Maps. The Abscissa Represents Doppler Frequency in Hz, and the Ordinate is Doppler Response in dB. The Dotted Curves are the Doppler Responses Without Self-Cohering. The Solid Curves are the Doppler Responses After Self-Cohering Using the ISCA + ITCA.

45
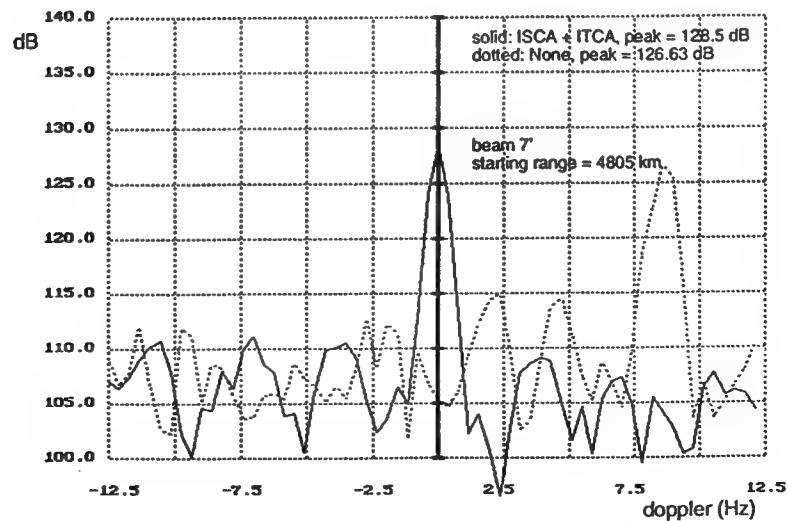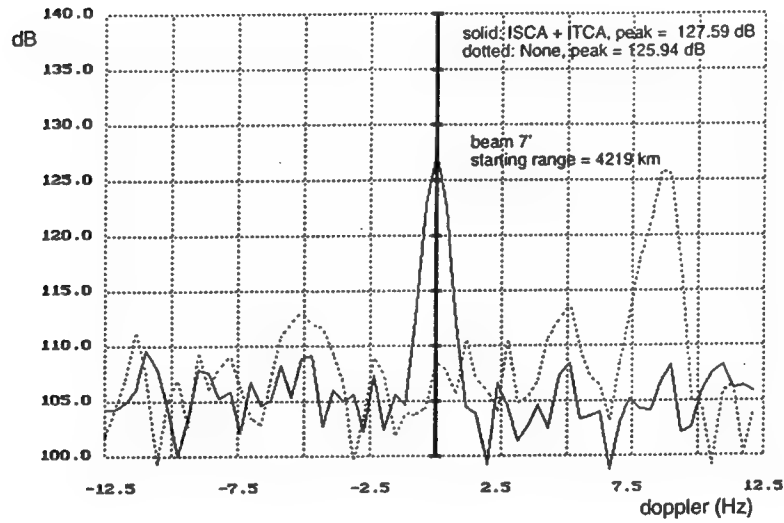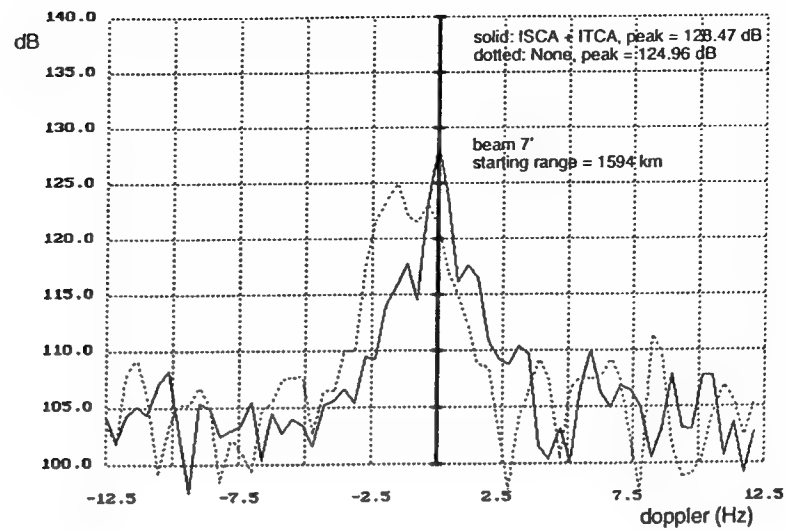
Figure 5.20.　(continued).

46

5.5. Processing Results for the Nov01506 Data Set

5.5.1. Data Description

The data set labeled Nov01506 furnished by Rome Laboratory was similar, in terms of format and ionospheric conditions, to the Nov01504 data described in Section 5.3. A minor format difference was that the current data consisted of 80 sweeps instead of 81. As before, a nonlinear correction was introduced into the sequence of frequency samples, improving the range resolution by 90% (16 km instead of 30 km). The Nov01506 data set was collected 6 minutes after the Nov01504 data under nearly identical ionospheric conditions.

5.5.2. Results

Figure 5.21 shows the results of applying spatial and temporal corrections to the Nov01506 data set. Subarray processing was applied spatially and ITCA was used temporally. The figure consists of range-Doppler-azimuth maps for beams 6' through 14', where the corrected beam position $b' = b + 2.6$ degrees and b is the original beam position as explained in Section 4.2. The horizontal axis of each strip spans the Doppler interval -12.5 to 12.5 Hz. On the vertical axis, range starts at 0 km at the top of each strip. The range bin segment is $\Delta N_r = 5$, and the sweep segment is $\Delta N_s = 32$.

The upper sequence of maps in Figure 5.21(a) shows the original data without corrections. The bright spot at zero range is due to the transmitter groundwave. As expected, it is strongest at beam 11' and appears in other beam positions through the azimuth sidelobes. Notice that the displayed gray scale does not accommodate the transmitter signal at beam 11' which drives the scale into saturation. Because of the transmitter-based sweep-to-sweep pre-calibration discussed in Section 3, the first range cell exhibits the ideal Hamming windowed Doppler response. As in Figure 5.17(a), the vertical lobe at zero Doppler in beam 11' is due to leakage of the groundwave through range sidelobes.

The lower sequence of maps of Figure 5.21(b) shows the same data after spatial and temporal corrections were applied. Within the main ground backscatter region, at about one-third of the displayed range interval, significant reduction in Doppler spread can be seen in beams 6' through 9' and in beam 13'. An average increase in gain of about 3 dB was observed in these beam positions, whereas gain increases of 5.5 dB to 6.5 dB were common.

Figure 5.21(a) shows the regions of spread-Doppler clutter beyond the transmitter footprint. As in the earlier Nov01504 data set, self-cohering performed remarkably well in these regions. The resulting improvements can best be seen in beams 7' through 10'. In these regions, the main response at zero Doppler was restored to its theoretical width, and gain improvements ranged between 4 and 10.4 dB with an average of 6 dB.
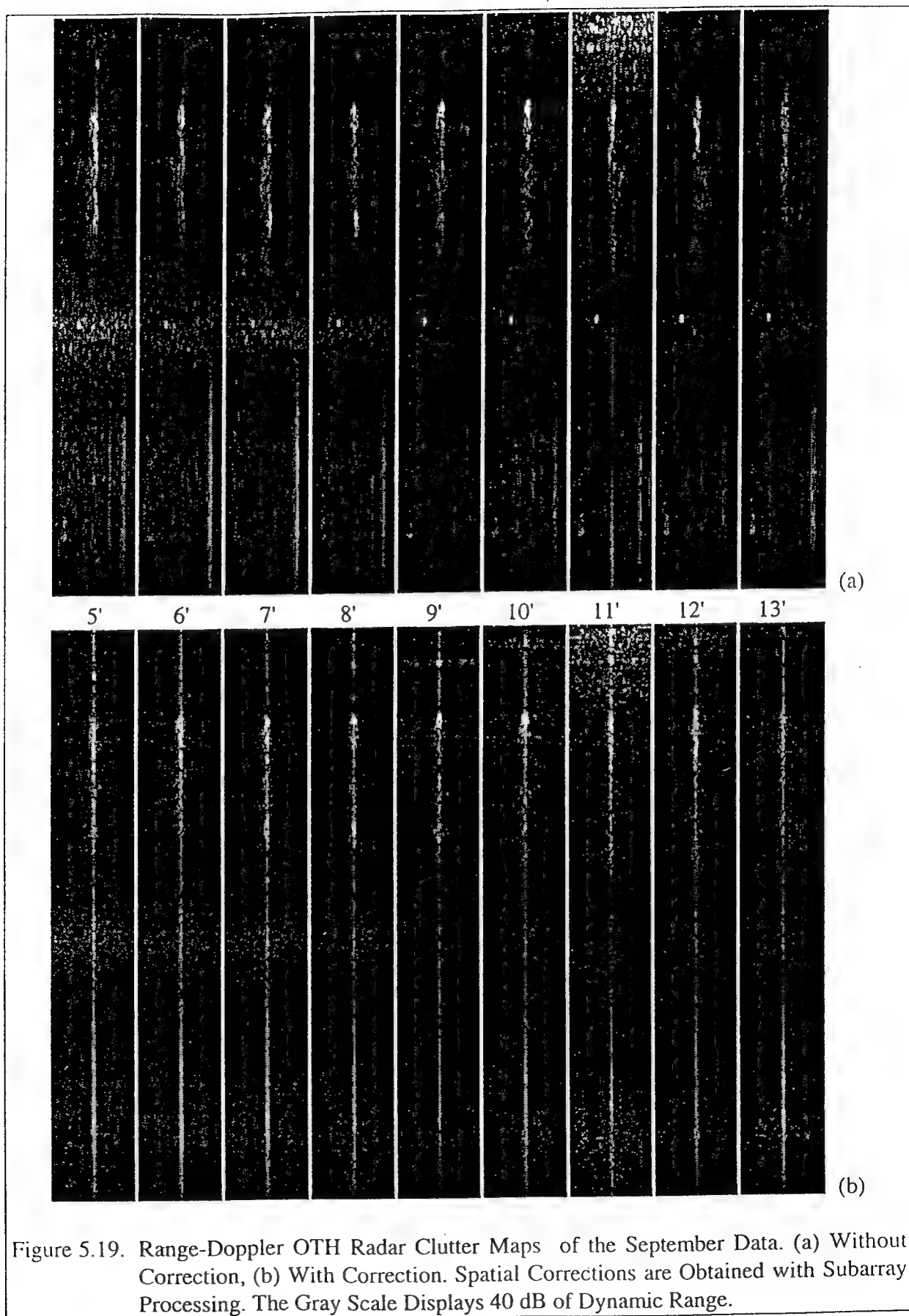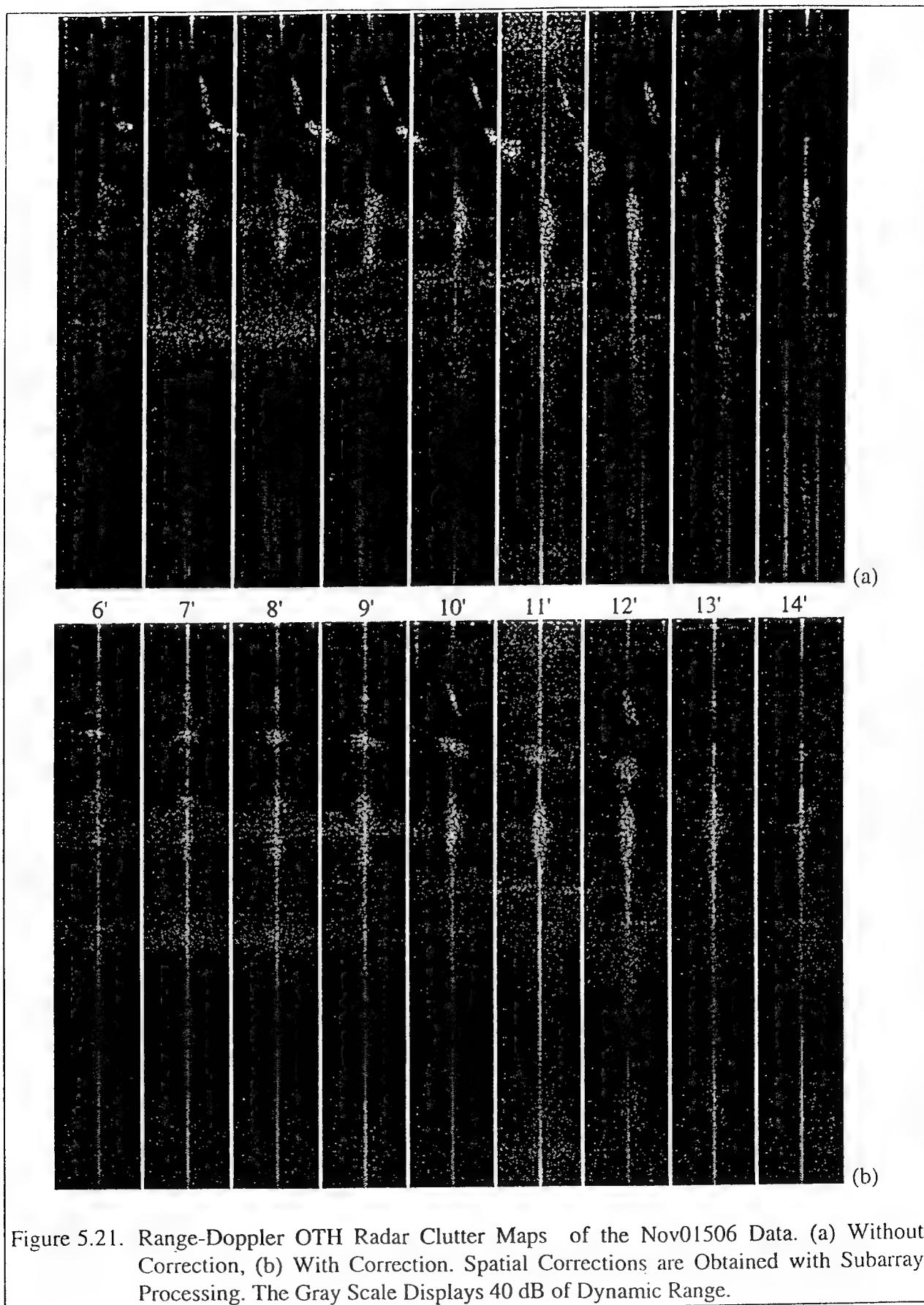
47

Figure 5.21. Range-Doppler OTH Radar Clutter Maps of the Nov01506 Data. (a) Without Correction, (b) With Correction. Spatial Corrections are Obtained with Subarray Processing. The Gray Scale Displays 40 dB of Dynamic Range.

5.6. Retaining the Absolute Doppler Shift

By analogy with losing the absolute azimuth position after direct application of the spatial correction, as described in Section 4.2, the mean Doppler shift is also automatically removed at all ranges after applying the temporal correction. This has no effect on ground backscatter because its true mean Doppler shift is zero to start with. In an OTH radar application, ground backscatter will always exist in the same range interval being searched for targets and the way we presented the results so far is completely adequate for this purpose. However, when returns from ionospheric irregularities lose their mean Doppler shift, information critical to ionospheric propagation studies is lost. The new method of phase unwrapping, described in Section 4.3, is used here to estimate the linear phase term in the temporal, sweep-to-sweep phase corrections so that ionospheric returns can be registered at their absolute Doppler after self cohering.

Figure 5.22 shows the results of applying this procedure to the Nov01504 data set. Figure 5.22(a) shows the data before correction, and is identical to Figure 5.17(a). Figure 5.22(b), where the absolute Doppler shift is retained is retained, should compare with Figure 5.17(b). Notice that most of the returns from ionospheric disturbances are correctly registered. As discussed in Section 4.3, the new method of phase unwrapping is not completely error free. For example, if phase corrections vary rapidly over the full 2π interval, trying to estimate a linear phase term would be meaningless. An example of this situation can be seen in the spread-Doppler clutter region where the underlying temporal phase error pattern introduced by the ionosphere is fairly random, resulting in the large spread in Doppler characteristic to this region. Based on the original range-Doppler-azimuth map of Figure 5.22(a), identifying a mean Doppler shift in the spread-Doppler clutter region by simply looking at the map is not possible. Knowing that such returns are due to ground backscatter, the best strategy is not to attempt any temporal phase unwrapping in this region as we did in Figure 5.17(b).

Notice that within the spread-Doppler clutter region of Figure 5.22(b), random Doppler shift is introduced every $\Delta N_r = 5$ range bins; i. e., wherever the temporal phase unwrapping procedure is applied. Except for these shifts, Figures 5.17(b) and 5.22(b) should compare with each other.

It should be noted that the self cohering procedure developed in this study applies only to ground backscatter. In most of the range-Doppler-azimuth maps presented in this report, the algorithms were applied to large range intervals containing both ground backscatter and direct returns from ionospheric irregularities. As expected, no measurable improvements were achieved on the ionospheric returns, which is consistent with the underlying theory. However, processing large range intervals made it possible to find the very interesting regions of spread-Doppler clutter where dramatic improvements were obtained.

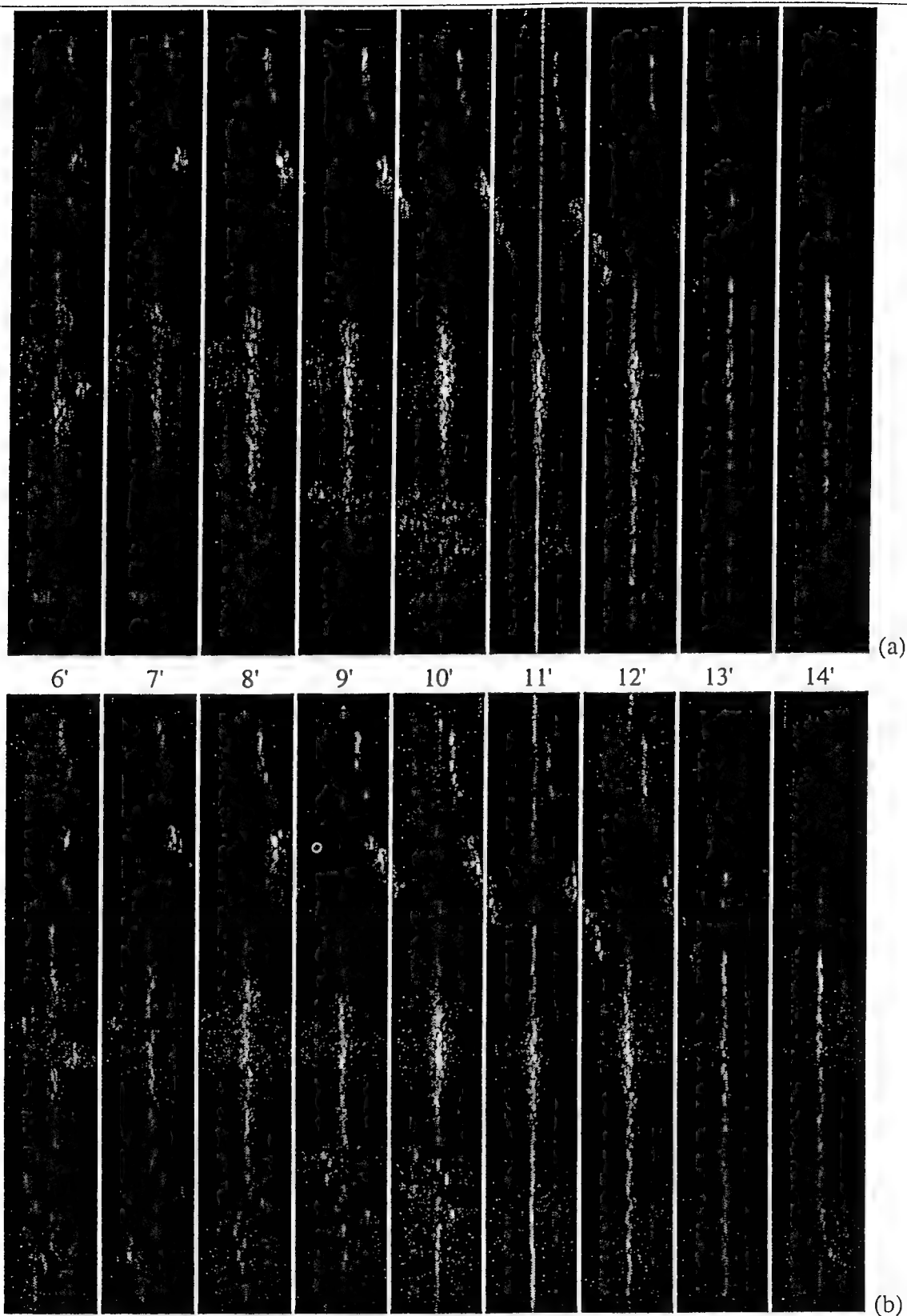6'   7'   8'   9'   10'   11'   12'   13'   14'

(a)

(b)

Figure 5.22. Range-Doppler OTH Radar Clutter Maps from the Nov01504 Data. (a) With Temporal and Spatial Corrections. Mean Doppler Shift is Removed. The Gray Scale Displays 40 dB of Dynamic Range. (b) Mean Doppler Shift is Retained.

5.7. Applying Processing Algorithms to Simulated Noise

To test our processing algorithms against the production of phantom results not supported by the data, we simulated Doppler-range maps based on a data file containing independent, identically-distributed, Gaussian random noise samples as shown in Figure 5.23. Each strip is a Doppler-range map in the format of Figure 5.17. A dynamic range of 17.5 dB is displayed. Figure 5.23(a) shows the resulting map when no corrections are applied. As expected, the Doppler is spread over the full 25 Hz band. In Figures 5.23(b-f), the number of sweeps $\Delta N_s = 32$ is kept constant while the choice of algorithm and ΔN_r are both varied.

In Figures 5.23(b-d), the number of range bins $\Delta N_r = 5$ is fixed, and the algorithm changes. In Figure 5.23(b), temporal corrections only are used, leading to a noticeable reduction in Doppler spread. This is due to the small sample size, $\Delta N_r = 5$, since non-zero amounts of cross-correlation inevitably exist over any set of 5 range bins. In Figure 5.23(c), spatial corrections only are applied. As expected, no change in Doppler spread is found because the data are less correlated from sweep to sweep over the larger 64-sweep interval processed. Figure 5.23(d) shows the results of applying both temporal and spatial corrections, with the resulting Doppler spread being similar to that of Figure 5.23(b). Clearly, spatial processing does not affect the results.

In Figures 5.23(e) and 5.23(f) the size of range bin segment is increased to $\Delta N_r = 10$ and $\Delta N_r = 20$, respectively. Notice the widening in Doppler as ΔN_r increases, which is to be expected as the range cross-correlation tends to zero with increasing sample size. While increasing ΔN_r to 10 or 20 in the actual VALAR OTH data would help suppress phantom correlations, it is incompatible with the physics of the problem because of the coarse range resolution available and the limited spatial extent of the irregularities. An OTH radar with finer range resolution, such as the WARF, has the potential to show greater improvement in performance.
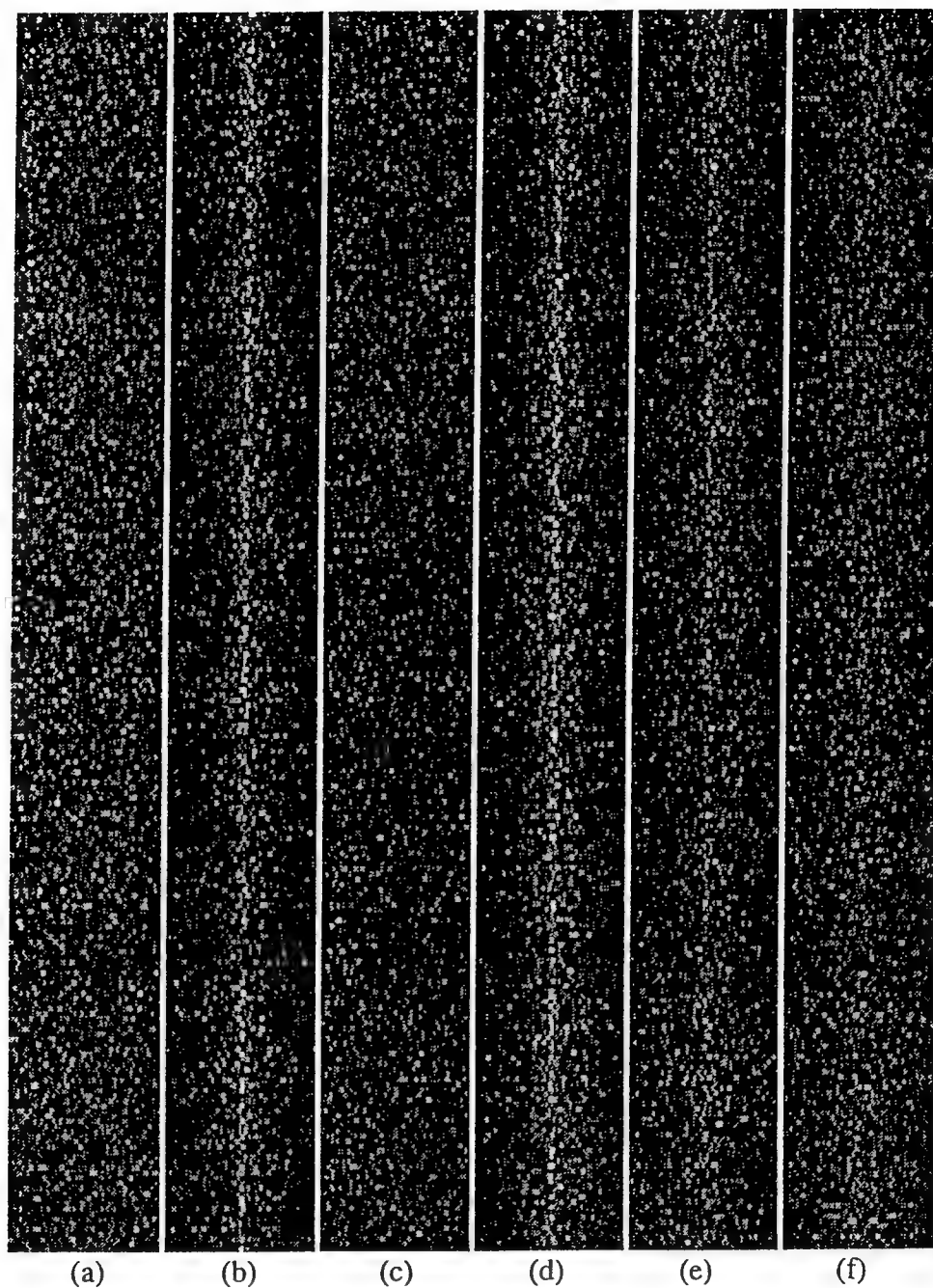
51

Figure 5.23. Doppler-Range Maps of Simulated Noise. (a) No Corrections. (b) Temporal Corrections Only with $\Delta N_r = 5$. (c) Spatial Corrections Only with $\Delta N_r = 5$. (d) Temporal and Spatial Corrections with $\Delta N_r = 5$. (e) Temporal and Spatial Corrections with $\Delta N_r = 10$. (f) Temporal and Spatial Corrections with $\Delta N_r = 20$.

6. CONCLUSIONS

We have experimentally evaluated the feasibility of self cohering on clutter by examining the OTH Doppler clutter response of the VALAR system for three data sets furnished by Rome Laboratory. The results indicate that the limitations on resolution imposed by random fluctuations of the ionospheric medium can be overcome. Most beam positions in the data sets exhibited some noticeable reduction in Doppler spread. The results show wide variation between data sets, and as a function of range within a data set. The more severe the distortion, the greater the improvement. By applying a combination of spatial and temporal correlation algorithms, gain improvements up to 10 dB were achieved. Doppler spread was usually reduced to some extent, and in one case where clutter Doppler was spread over the full unambiguous Doppler band before processing, it was confined to dc after processing. Spread-Doppler clutter was, in this instance, reduced below the noise, corresponding to a 10 to 12.5 dB increase in sublclutter visibility.

The algorithms were not effective when the bandwidth was decreased from 10 to 5 kHz. Processing gains increased by only one or two dB. We conclude that wider bandwidths and larger receive arrays should improve algorithm performance by providing finer resolution of the ionospheric irregularities. This would allow one to come close to recovering the error-free antenna pattern and Doppler spectrum. The potential improvement should be almost equal to the degradation.

Spatial correlation and related algorithms were applied to clutter returns from over the horizon radar to generate corrections that calibrate the receive propagation path. The results show that:

(1) Beam spreading effects can be compensated using distributed clutter
(2) Compensation can be achieved within the coherence time of the medium
(3) Compensation reduces spread-Doppler clutter
(4) Doppler spreading effects can be compensated using returns from distributed clutter by means of a Temporal Correlation Algorithm (TCA) that operates on a sequence of radar sweeps at the beamformed output in a manner similar to the way its spatial counterpart (SCA) operates on array element, or subarray, data.
(5) Combined use of the SCA and TCA provides even greater array processing gain, less Doppler spread, and lower Doppler sidelobes.

We have thus shown that an OTH radar cab be spatially and temporally self cohered based on radar returns without the use of a beacon or other phase synchronizing source that would have to be placed in the vicinity of expected radar targets. The process increases subclutter visibility, narrows Doppler resolution, and extends the spatial coherence across the receive aperture to recover degraded angular resolution.

The primary implications are:

(1) It is possible to build OTH radars that have much finer angular and Doppler resolution than current systems with greater subclutter visibility
(2) Performance of existing OTH radars can be substantially improved by using the processing techniques considered in this report.

For future systems, Doppler resolution can be improved by increasing the dwell time, and angle resolution can be improved by increasing the aperture size. Since the spatial correlation techniques will correct for element position errors, and, in fact, any element-to-element mechanical or electrical errors, while correcting for the errors induced by the ionosphere, rapidly reloctable OTH radars, with minimum site preparation, become feasible. For existing systems, in which element level data is not available, performance improvement can be obtained by use of the Temporal Correlation Algorithm (TCA) at the beamformed output, provided I and Q data are made available.

7. RECOMMENDATIONS FOR FUTURE WORK

Because of the importance of these techniques to OTH radar and HF communications, it is necessary that their analysis, development, and experimental evaluation continue. Additional sources of OTH radar data, such as the MITRE high-resolution bistatic OTH radar research facility in Texas, or SRI's high resolution WARF radar on the West Coast, should be considered. Once an evaluation of the adaptively beamformed pattern using the Goosebay beacon data is completed, additional experiments should be undertaken using remote HF radios. The VALAR radar should be used in conjunction with HF radios to develop applications to communications. The VALAR receive array could be used as the antenna for a central HF communications facility to communicate with remote radios in instances of severe ionospheric turbulence.

Self calibration and/or self cohering is one of two major aspects of adaptive receiver beamforming. In Reference [29], GORCA demonstrated that directional interference can be attenuated prior to self cohering, thereby improving the performance of the self cohering process as well as the radar performance. Experiments should be conducted to verify this in the HF OTH environment. The recently developed orthogonal projection method [27, 29-34], for example, could be used to eliminate interference due to lightning as well as other non-intentional and intentional HF interference sources. Other experiments, involving a moving target or an additional beacon should be conducted, and methods to maximize angular estimation accuracy should be considered.

Now that the problem of compensating for receiver beam spreading has been mitigated, the problem of transmitter beam spreading must also be addressed. For instance, can the elements of a transmitter array be phased such that the OTH transmitted beam is optimized? Some form of closed-loop procedure based on the received OTH clutter returns would be needed. Thus far, only dominant scatterer type algorithms have been demonstrated for two-way self cohering [35, 36]. Can this be done in real time, using spatial correlation type algorithms to achieve two-way cohering based on OTH clutter returns?

Before these additional problems are investigated, processing of data using the Goosebay beacon, or some other remote HF transmitter, as a target is necessary to measure the array's angular response and to determine the angular resolution and sidelobe level with and without self cohering. In addition to using the beacon as a target to evaluate the pattern, the array could also be self cohered using the beacon as a phase synchronizing source, and the resulting phase corrections could be compared with those obtained by cohering on clutter. The requirements for performing this validation and further evaluation of the self cohering results are discussed below.

55

7.1. Beacon Requirements and Processing Plans

The OTH beacon signal should originate from approximately the same time and place as the ground clutter returns, but it should be distinguishable from them. The beacon should have a swept frequency waveform similar to the Ava transmission, and its transmissions should be timed to overlap the arrival of the Ava signal at Goosebay. Its sweep should be timed so that the receiver FFT places it at a range different from the Ava range, the auroral backscatter range, and the actual Goosebay OTH clutter range. In addition, a known Doppler offset should be introduced to simulate a moving target. A 10-Watt ERP should provide adequate signal-to-clutter ratio, and 0.5 degree rms phase stability relative to the receiver LO should provide Doppler sidelobes well below noise.

We intend to use the beacon as a point target to measure angular and Doppler response with and without self cohering on clutter. In addition, we will compare phase corrections derived from the beacon to those derived from the clutter in the vicinity of the beacon. We will also determine how far we can steer in range and azimuth after cohering, by cohering on clutter at a range and/or azimuth offset from the beacon, or "target," position.

8. REFERENCES

[1] P. R. Franchi and E. J. Tichovolsky, *Phase Screen Modulation as a Source of Clutter Related Noise in Over-The-Horizon Radar*, Technical Report RADC-TR-89-296, Rome Air Development Center, Rome, N.Y., 1989.

[2] J. Thomason, Chairman, Session 2A: HF Over-the-Horizon Radar, *Proc. Seventh International Ionospheric Effects Symposium*, Alexandria, VA, May 4-6, 1993.

[3]   B. D. Steinberg and H. Subbaram, *Microwave Imaging Techniques*, Wiley, New York, 1992.

[4] B. D. Steinberg, *Microwave Imaging with Large Antenna Arrays*, Wiley, N. Y., 1983.

[5] D. S. Choi, B. Weijers, R. J. Norris and N. B. Meyers, The Spatial and Temporal Characteristics of High Frequency Auroral Backscatter, *AGARD Conference Proceedings 528 on Radiolocation Techniques*, London, June 1-5, 1992.

[6] V. I. Tatarski, *Wave Propagation in a Turbulent Medium*, Translated from Russian by R. A. Silverman, McGraw Hill, N.Y., 1961.

[7] S. H. Taheri and B. D. Steinberg, "A Measurement System and Analysis Procedure for Determining the Spatial Phase Structure Function of Ionospherically Reflected Waves", *IEEE Trans. Antennas and Propagation*, AP-27(4), pp. 500-501, July 1979.

[8] B. D. Steinberg, "A Proposed Approach for Increasing the Azimuthal Resolution of HF Radar", *IEEE Trans. Antennas and Propagation*, AP-20(5), pp. 613-618, Sept. 1972.

[9] R. L. Fante and S. Dhar, *A Model for Target Detection in Over the Horizon Radar*, Mitre Technical Report MTR 10510, Prepared for ESD under contract F19628-89-C-0001, Nov. 1988.

[10] R. L. Fante, *A Model for Target Detection: Effect of Ionospheric Fluctuations*, Mitre Technical Report MTR 10541, Prepared for ESD under contract F19628-89-C-0001, Feb. 1989.

[11] H. G. Booker, J. W. Tao and B. Behroozi-Toosi, "A Scintillation Theory of Fading in Long Distance HF Ionospheric Communications", *Journal of Atmospheric and Terrestrial Physics*, 49(9), pp. 939-958, Sept. 1987.

[12] B. D. Steinberg, "Radar Imaging from a Distorted Array: The Radio Camera Algorithm and Experiments," *IEEE Trans. Antennas Propag.*, pp. 740-748, Sept. 1981.

[13] E.H. Attia and B.D. Steinberg, "Self-Cohering Large Antenna Arrays Using The Spatial Correlation Properties of Radar Clutter," *IEEE Trans. Antennas and Propagation*, Vol. AP-37, No. 1, pp. 30-38, January 1989.

[14] E.H. Attia, "Phase Synchronizing Large Antenna Arrays Using the Spatial Correlation Properties of Radar Clutter," *Proc. National Radio Science Meeting (URSI)*, Boulder, Colorado, pp. 105, January 1984.

[15] E. H. Attia, *Phase Synchronizing Large Antenna Arrays Using The Spatial Correlation Properties of Radar Clutter*, Ph. D. Thesis, The Moore School of Electrical Engineering, University of Pennsylvania, 1984.

[16] H. Subbaram and B.D. Steinberg, "A Scene-Independent Technique for Self-Calibrating Phased Arrays in a Coherent Target Environment," *Proc. 1987 URSI Radio Science Meeting*, Virginia Polytech. Inst., Blacksburg, VA, June 1987.

[17] K. Abend, E. Stockburger, and J. McAteer, "Auto-Focus/Motion-Compensation for Radar Imaging," *Joint-Service Combat Identification Systems Conf. (CISC-90)*, Naval Post

Graduate School, Monterey, Calif., December 1990.

[18] K. Abend, E.H. Attia, and B. Fell *Autofocus Algorithm Applied to SAR Imagery*, Final Technical Report prepared by GORCA for McDonnell Douglas Corp., New Aircraft Products Division, St. Louis, MO, August 1992.

[19] E.H. Attia, "Statistics of the Power Pattern of a Periodic Array Self-Cohered using the SCA," *11th annual Benjamin Franklin Symposium on Antenna and Microwave Technology in the 1990s*, Symposium Digest pp 108-111, May 1, 1993, Valley Forge, PA.

[20] E.H. Attia, *Large Coherent Arrays for Laser Radars*, Phase I Final Report, Contract No. N00014-91-C-0150, prepared by *Interspec, Inc.* for ONR/SDIO, November, 1991.

[21] J.R. Fienup, "Phase Error Correction by Shear Averaging," Signal Recovery and Synthesis III, Topical Meeting, 14-16 June 89, 1989 Technical Digest Series, Vol. 15, *Optical Soc. of Am.*, Washington, DC.

[22] P. Eichel, D. Ghiglia, and C. Jakowatz, Jr., "Speckle Processing Method for Synthetic-Aperture-Radar Phase Correction," *Optics Letters*, Vol. 14, No. 1, pp. 1-3, January 1, 1989.

[23] E. H. Attia, *Self-Cohering Airborne Distributed Arrays*, R&D Final Report prepared by Interspec for Rome Laboratory, Hanscom AFB, MA, Contract No. F19628-C-0080, Report No. RADC-TR-88-109, June 1988.

[24] E.H. Attia, "Self-Cohering Airborne Distributed Arrays Using the Robust Minimum Variance Algorithm," *IEEE AP-S and URSI International Symposium*, Philadelphia, Symposium Digest, vol 2, pp. 603-606, June 1986.

[25] B. Kang, H. Subbarram, and B.D. Steinberg, "Improved Adaptive-Beamforming Target for Self-Calibrating a Distorted Phased Array," *IEEE Trans. Antennas and Propagation*, Vol. AP-38, No. 2, pp. 186-194, February 1990.

[26] J. Tsao, "Phased Array Beamforming by the Parceval's Theorem," *IEEE AP-S and URSI International Symposium*, Philadelphia, Symposium Digest, vol 1, pp. 335-338, June 1986.

[27] H. Subbaram, K. Abend, L. Martinson, and H. Attia, *Integrated Design of Smart Phased Array Systems*, Phase I SBIR Final Report, Contract No. F19628-89-C-0179, Rome Laboratory, Hanscom AFB, March 1990.

[28] N. Morrison, *Introduction to Sequential Smoothing and Prediction*, McGraw-Hill, New York, 1969.

[29] H. Subbaram, K. Abend, E.H. Attia, E. Stockburger, and B. Fell, *Integrated Design of Smart Phased Array Systems*, Phase II SBIR Final Report under Contract No. F19628-89-C-0179, Report RL-TR-92-285, Rome Laboratory, Griffiss AFB, N.Y., Dec. 1992.

[30] H. Subbaram, K. Abend, H. Attia, E. Stockburger and B. Fell, *Integrated Design of Smart Phased Array Systems*, Phase II SBIR Final Technical Report No. RL-TR-92-285, Rome Laboratory, Griffiss AFB, N. Y., Dec. 1992.

[31] H. Subbaram and K. Abend, "Interference Suppression via Orthogonal Projections: A Performance Analysis," *IEEE Trans. on Antennas and Propagation*, Vol. 41, No. 9, pp. 1187-1194, September 1993.

[32] K. Abend and H. Subbaram, "Orthogonal Projection Technique (OPT) for Adaptive Interference Suppression," presented at the *ASTP Working Group Meeting*, Rome Laboratory, Griffiss AFB, N.Y., May 1992.

[33] K. Abend and H. Subbaram, "Interference Suppression via Orthogonal Projections," *Proc. IEEE Sixth SP Workshop on Statistical Signal and Array Processing*, Victoria, B.C., Canada, pp. 239-242, October 1992.

[34] K. Abend et. al., *Sidelobe Reduction and Clutter Suppression for a Distributed Sparse Array Radar System*, Phase 1 SBIR Final Report on Contract No. F29601-88-C-0089 for USAF Weapons Laboratory / TAS, Kirtland AFB, NM., July 1989.

[35] E. H. Attia and K. Abend, "An Experimental Demonstration of a Distributed Array Radar," *Proc. IEEE AP-S International Symposium Digest*, London, Ontario, pp. 1720-1723, June 1991.

[36] E. H. Attia, K. Abend, et. al., *Distributed Array Radar Demonstration*, Interspec Phase II SBIR Final Report on Contract No. F19628-87-C-0136 for Rome Lab, Hanscom A.F.B., MA, January 1990.

MISSION
OF
ROME LABORATORY

Mission. The mission of Rome Laboratory is to advance the science and technologies of command, control, communications and intelligence and to transition them into systems to meet customer needs. To achieve this, Rome Lab:

    a. Conducts vigorous research, development and test programs in all applicable technologies;

    b. Transitions technology to current and future systems to improve operational capability, readiness, and supportability;

    c. Provides a full range of technical support to Air Force Material Command product centers and other Air Force organizations;

    d. Promotes transfer of technology to the private sector;

    e. Maintains leading edge technological expertise in the areas of surveillance, communications, command and control, intelligence, reliability science, electro-magnetic technology, photonics, signal processing, and computational science.

The thrust areas of technical competence include: Surveillance, Communications, Command and Control, Intelligence, Signal Processing, Computer Science and Technology, Electromagnetic Technology, Photonics and Reliability Sciences.